

1 **Sea ice algorithms inter-comparison and evaluation:**  
2 **towards further identification of challenges and optimal**  
3 **approach using passive microwave observations**

4 **Natalia Ivanova<sup>1</sup>, Leif T. Pedersen<sup>2</sup>, Rasmus T. Tonboe<sup>2</sup>, Stefan Kern<sup>3</sup>, Georg**  
5 **Heygster<sup>4</sup>, Thomas Lavergne<sup>5</sup>, Atle Sørensen<sup>5</sup>, Roberto Saldo<sup>6</sup>, Gorm Dybkjær<sup>2</sup>,**  
6 **Ludovic Brucker<sup>7, 8</sup>, and Mohammed Shokr<sup>9</sup>**

7

8 (1){Nansen Environmental and Remote Sensing Center, Bergen, Norway}

9 (2){Danish Meteorological Institute, Copenhagen, Denmark}

10 (3){University of Hamburg, Hamburg, Germany}

11 (4){University of Bremen, Bremen, Germany}

12 (5){Norwegian Meteorological Institute, Oslo, Norway}

13 (6){Technical University of Denmark, Lyngby, Denmark}

14 (7){NASA Goddard Space Flight Center, Cryospheric Sciences Laboratory, Code 615,  
15 Greenbelt, Maryland 20771, USA}

16 (8){Universities Space Research Association, Goddard Earth Sciences Technology and  
17 Research Studies and Investigations, Columbia, Maryland 21044, USA}

18 (9){Environment Canada, Ontario, Canada}

19

20 Correspondence to: N. Ivanova ([natalia.ivanova@nersc.no](mailto:natalia.ivanova@nersc.no))

21

22

23

24

25

26

## 1 **Abstract**

2 Sea ice concentration has been retrieved in Polar Regions with satellite microwave  
3 radiometers for over 30 years. However, the question remains open, what is the optimal sea  
4 ice concentration retrieval method for climate monitoring. This paper presents some of the  
5 key results of an extensive algorithm inter-comparison and evaluation experiment. Thirty sea  
6 ice algorithms entered the experiment where their skills were evaluated systematically over  
7 low and high sea ice concentrations; thin ice and areas covered by melt ponds. A selection of  
8 thirteen algorithms is shown in the article to demonstrate the results. Based on the findings, a  
9 hybrid approach is suggested to retrieve sea ice concentration globally for climate monitoring  
10 purposes. This approach consists of a combination of two algorithms, dynamic tie points  
11 implementation, and atmospheric correction of input brightness temperatures. The method  
12 minimizes inter-sensor calibration discrepancies and sensitivity to error sources with seasonal  
13 to inter-annual variations and potential climatic trends, such as atmospheric water vapour and  
14 water surface roughening by wind.

15

## 16 **1 Introduction**

17 From a perspective of climate change, it is important to know how fast the total volume of sea  
18 ice is changing. In addition to sea ice thickness (Kern et al., 2015), this requires reliable  
19 estimates of sea ice concentration (SIC). Consistency in sea ice climate records is crucial for  
20 understanding of internal variability and external forcing (e.g. Notz and Marotzke, 2012) in  
21 the observed sea ice retreat in the Arctic (Cavalieri and Parkinson, 2012) and expansion in the  
22 Antarctic (Parkinson and Cavalieri, 2012).

23 Accuracy and precision serve as measures of performance of a SIC algorithm. Accuracy  
24 (expressed by bias) is the difference between the mean retrieval and the true value. Precision  
25 (expressed by standard deviation, SD) is the range within which repeated retrievals of the  
26 same quantity scatter around the mean value (see also Brucker et al., 2014, where precision is  
27 addressed in detail). Average accuracy of commonly known algorithms, such as NASA Team  
28 (Cavalieri et al., 1984) and Bootstrap (Comiso, 1986), is reported to be within  $\pm 5\%$  in winter  
29 in a compact (high concentration) ice pack. Accuracy of the Bootstrap scheme applied to  
30 AMSR-E (Advanced Microwave Scanning Radiometer for Earth Observing System) data,  
31 expressed as standard deviation of the scatter around the ice line, was estimated at 2.5%. The  
32 accuracy including combined effect of surface temperature and emissivity variability was 4%

1 (Comiso 2009). A comparison of seven algorithms to a trusted dataset of Synthetic Aperture  
2 Radar (SAR) and ship-based observations in the Arctic showed precision of 3–5%, including  
3 sensor noise (Andersen et al., 2007). In summer and at the ice edge the retrievals are more  
4 uncertain, and accuracy can be as poor as  $\pm 20\%$  (Meier and Notz, 2010). Inter-comparison of  
5 eleven SIC algorithms in the Arctic showed differences in SIC retrievals of 2.0–2.5% in  
6 winter in the areas of consolidated ice (5–12% for intermediate SIC) and 2–8% in summer  
7 reaching up to 12% in the Canadian Archipelago area (Ivanova et al., 2014). The large  
8 uncertainty in retrievals of the summer period is caused by increased variability in sea ice  
9 emissivity due to the surface wetness and presence of melt ponds. Part of the uncertainty at  
10 low and intermediate SICs, which is relevant both for summer and for the marginal ice zone  
11 at any time, is caused by atmospheric contributions and wind roughening of open water areas,  
12 as shown for the Arctic by Andersen et al. (2006). Marginal ice zone is characterized by  
13 increased uncertainties due to smearing and footprint mismatch effects. The uncertainties over  
14 consolidated ice during Arctic winter were explained by variations in sea ice emissivity  
15 (Andersen et al., 2007).

16 In this study we focus on the following four error sources, to which the algorithms have  
17 different responses: 1) sensitivity to emissivity and physical temperature of sea ice, 2)  
18 atmospheric effects, 3) melt ponds, and 4) thin ice. The sensitivity to emissivity and physical  
19 temperature of sea ice depends on the selection of input brightness temperatures (Tbs)  
20 available at electromagnetic frequencies between 6 and near 90 GHz in vertical (V) and  
21 horizontal (H) polarisations, and the method applied to retrieve SIC from them, which  
22 distinguishes each algorithm among the others (explained in Sect. 2.1). Kwok (2002) and  
23 Andersen et al. (2007) showed that SIC algorithms do not reflect the near 100% ice  
24 concentration variability in the Arctic adequately. Variability due to actual ice concentration  
25 changes in the order of less than 3% is below the noise floor of the algorithms. Heat and  
26 moisture fluxes between the surface (ocean or ice) and the atmosphere are sensitive to small  
27 variations in the near 100% ice cover (Marcq and Weiss, 2012). This unresolved SIC  
28 variability can thus be of significant importance for sea ice models (and consequently coupled  
29 climate models) when assimilating these data without proper handling of the uncertainties.  
30 The apparent fluctuations in the derived ice concentration in the near 100% ice regime are  
31 primarily attributed to snow/ice surface emissivity variability around the tie point (predefined  
32 Tb for ice) and only secondarily to actual SIC fluctuations (Andersen et al., 2007).

1 The second error source is represented by atmospheric effects, such as water vapour, cloud  
2 liquid water (CLW) and wind roughening of the water surface. It causes the observed  $T_b$  to  
3 increase and to change as a function of polarisation and frequency, season and location  
4 (Andersen et al., 2006). This effect is usually larger during summer and early fall and over  
5 open water (also in the marginal ice zone) because of the larger amounts of water vapour and  
6 CLW in the atmosphere, and generally more open water areas present.

7 Algorithms with different sensitivities to surface emissivity and atmospheric effects produce  
8 different estimates of trends in sea ice area and extent on seasonal and decadal time scales  
9 (Andersen et al., 2007). Effect of diurnal, regional and inter-annual variability of atmospheric  
10 forcing on surface microwave emissivity was also reported in a model study of Willmes et al.  
11 (2014). This means that not only sea ice area has a climatic trend, but atmospheric and surface  
12 parameters affecting the microwave emission may also have a trend. Such parameters can be  
13 wind patterns, atmospheric water vapour and CLW (Wentz et al., 2007), snow depth and  
14 snow properties, and the fraction of multiyear ice (MYI).

15 However, some algorithms are less sensitive than others to these effects (Andersen et al.,  
16 2006; Oelke, 1997), and it is thus important to select an algorithm with low sensitivity to  
17 them. It is particularly important to have low sensitivity to error sources, which it is currently  
18 impossible to correct for, e.g. extinction and emission by CLW or sea ice emissivity  
19 variability. We therefore designed a set of experiments to test a number of aspects related to  
20 SIC algorithm performance, ultimately to allow us to select an optimal algorithm for retrieval  
21 of a SIC climate data record.

22 Melt ponds on Arctic summer sea ice represent an additional source of errors due to their  
23 microwave radiometric signatures being similar to open water. Virtually all SIC algorithms  
24 based on the passive microwave channels around 19, 37, and 90 GHz are very sensitive to  
25 presence of melt water on the ice. The penetration depth of microwave radiation into liquid  
26 water is a few millimetres at most (Ulaby et al., 1986), and therefore it is impossible to  
27 distinguish between ocean water (in leads) and melt water (on the ice). This is the primary  
28 reason why most SIC algorithms are less reliable during summer and potentially  
29 underestimate the actual SIC (Fetterer and Untersteiner, 1998; Cavalieri et al., 1990; Comiso  
30 and Kwok, 1996). Melt ponds may exhibit a diurnal cycle with interchanging periods of open  
31 water and thin ice. This further complicates the SIC retrieval using satellite microwave  
32 radiometry during summer and increases the level of uncertainty. Some SIC algorithms have

1 been shown to underestimate SIC by up to 40% in the areas with melt ponds (Rösel et al.,  
2 2012b).

3 Thin ice is known to be another challenge for the passive microwave algorithms as they  
4 underestimate SIC in such areas (Heygster et al., 2014; Kwok et al., 2007; Cavalieri, 1994).  
5 Recent studies of aerial (Naoki et al., 2008) and satellite (Heygster et al., 2014) passive  
6 microwave measurements show an increase in  $T_b$  with sea ice thickness (<30 cm), which is  
7 more pronounced for lower frequencies and horizontal polarisation. Since an instantaneous  
8 amount of thin ice can reach as much as 1 million km<sup>2</sup> (total amount globally, Grenfell et al.,  
9 1992), the effect of SIC underestimation can be significant for ice area estimates, air-sea heat  
10 and moisture exchange and modelled ice dynamics. It may also affect ice volume estimates. It  
11 is suggested that the dependency of  $T_b$  on the sea ice thickness is due to changes in near-  
12 surface dielectric properties caused, in turn, by changes of brine salinity with thickness and  
13 temperature (Naoki et al., 2008).

14 For the first time this many (thirty) SIC algorithms have been evaluated in a consistent and  
15 systematic manner including both hemispheres, and their performance tested with regard to  
16 high and low SIC, areas with melt ponds, thin ice, atmospheric influence and tie points; and  
17 covering the observing characteristics of the Scanning Multichannel Microwave Radiometer  
18 (SMMR), Special Sensor Microwave/Imager (SSM/I) and AMSR-E. The novelty of the  
19 presented approach to algorithm inter-comparison is in the implementation of all the  
20 algorithms with the same tie points, which helps avoiding subjective tuning, and without  
21 applying weather filters, which have their weaknesses (also addressed in this study). When  
22 evaluating the algorithms we have in particular focused on achieving low sensitivity to the  
23 error sources over ice and open water, performance in areas covered by melt ponds in summer  
24 and thin ice in autumn. We suggest that an optimal algorithm should be adaptable to: 1)  
25 dynamic tie points in order to reduce inter-instrument biases and sensitivity to error sources  
26 with potential climatological trends and/or seasonal and inter-annual variations and 2)  
27 regional error reduction using meteorological data and forward models.

28 The algorithms evaluation was carried out in the context of European Space Agency Climate  
29 Change Initiative, Sea Ice (ESA SICCI) and is described in the following sections. Sect. 2  
30 describes the algorithms and the basis for selection of the thirteen algorithms to be shown in  
31 the following sections. Sect. 3 describes the data and methods. Sect. 4 presents the main  
32 results of the work: algorithms inter-comparison and evaluation, suggested atmospheric

1 correction and dynamic tie points approach. All the input data and obtained results are  
2 collocated and composed into a reference dataset called round robin data package (RRDP).  
3 This is done in order to achieve equal treatment of all the algorithms during the inter-  
4 comparison and evaluation, as well as to provide an opportunity for further tests in a  
5 consistent manner. This dataset is available from the Integrated Climate Data Center (ICDC,  
6 <http://icdc.zmaw.de/1/projekte/esa-cci-sea-ice-ecv0.html>). The discussion and conclusions are  
7 provided in Sect. 5 and Sect. 6 respectively.

8

## 9 **2 The algorithms**

10 During the experiment we implemented 30 SIC algorithms and found that they form groups  
11 according to the selection of channels and how these are used in each algorithm. We also  
12 found that algorithms within each group had very similar sensitivities to atmospheric effects  
13 and surface emissivity variations. This is in agreement with sensitivity studies (Tonboe, 2010;  
14 Tonboe et al., 2011) using simulated Tbs generated by coupling a thermodynamic ice/snow  
15 model to the Microwave Emissivity Model for Layered Snow Packs. To avoid redundancy we  
16 only include here a selection of 13 sea ice algorithms (Table 1), which were chosen as  
17 representatives of the groups.

### 18 **2.1 Selected algorithms**

19 The first group of algorithms, represented by Bootstrap polarisation mode (BP, Comiso,  
20 1986), includes polarisation algorithms. These algorithms primarily use 19 or 37 GHz  
21 polarisation difference (difference between Tbs in vertical and horizontal polarisations of the  
22 same frequency) or polarisation ratio (polarisation difference divided by the sum of the two  
23 Tbs). The next group uses 19V and 37V channels and is represented here by CalVal (CV,  
24 Ramseier, 1991). Commonly known algorithms in this group are NORSEX (Svendsen et al.,  
25 1983), Bootstrap Frequency Mode (BF, Comiso, 1986) and UMass-AES (Swift et al., 1985).  
26 Bristol (BR, Smith, 1996) represents the group that uses both polarisation and spectral  
27 gradient information from the channels 19V, 37V and 37H. The NASA Team algorithm (NT,  
28 Cavalieri et al., 1984) uses polarisation ratio at 19 GHz and gradient ratio at 19V and 37V.  
29 ASI, a non-linear algorithm (Kaleschke et al., 2001), and Near 90 GHz linear (N90, Ivanova  
30 et al., 2013) use the polarisation difference at near 90 GHz, both based on Svendsen et al.  
31 (1987). These are also called near 90 GHz or high-frequency algorithms. ESMR, named after

1 the single channel 18H radiometer on board Nimbus-5 operating from 1972 to 1977 (e.g.  
2 Parkinson et al., 2004), and 6H (Pedersen, 1994) are one-channel algorithms using horizontal  
3 polarisation at 18/19 GHz and 6 GHz respectively. ECICE (Shokr et al., 2008) and NASA  
4 Team 2 (NT2, Markus and Cavalieri, 2000) represent a special class of more complex  
5 algorithms where more channels are used and additional data may be needed as input. Finally  
6 we consider combinations of algorithms (hybrid algorithms), where one of the algorithms is  
7 expected to have low sensitivity to atmospheric effects over open water, and the other is  
8 expected to have a better performance over ice. This group includes the NT+CV algorithm  
9 (Ivanova et al., 2013): an average of NT and CV, the CV+N90 algorithm (Ivanova et al.,  
10 2013): an average of N90 and CV, and the OSISAF algorithm (Eastwood (ed.), 2012): a  
11 weighted combination of BR over ice and BF over open water (note that BF is identical to  
12 CV). The Bootstrap algorithm is tested in its two modes separately for the reasons explained  
13 in Sect. 5.1.

14 All the algorithms were evaluated without applying open water/weather filter, since our aim  
15 was a comparison of the algorithms themselves. We consider performance of an open  
16 water/weather filter separately in Sect. 4.4.

## 17 **2.2 Tie points**

18 A necessary parameter for practically every algorithm is a set of tie points – typical Tbs of sea  
19 ice (100% SIC) and open water (0% SIC). Under certain conditions, such as wind-roughened  
20 water surface or thin sea ice, it is difficult to define a single tie point to represent the surface.  
21 In nature, Tb may have a range of variability for the same ice type or open water due to  
22 varying emissivity, atmospheric conditions, and temperature of the emitting layer. Therefore  
23 the scatter of retrieved SIC near the tie points, which correspond to 0% and 100%, may lead  
24 to negative or larger than 100% SICs. The ECICE algorithm uses the probability distribution  
25 of the radiometric observations from each surface, instead of a single tie point.

26 In order to obtain an unbiased comparison of the algorithms, we developed a special set of tie  
27 points (Appendix A) based on the RRDP for both hemispheres and for each of the three  
28 radiometers: AMSR-E, SSM/I and SMMR. This enabled us to compare the algorithms  
29 directly without biases between the algorithms caused by differences in tie points. The set of  
30 the RRDP tie points differs from the original tie points provided with the algorithms. This is  
31 caused by the fact that we use different versions of the satellite data, which may have

1 different calibrations. Also, the tie points published with the algorithms are typically valid for  
2 one instrument and need to be derived for each new sensor. In this study the RRDP tie points  
3 were used for all the algorithms except ASI, NASA Team 2 and ECICE where such  
4 traditional tie points were not applicable, and therefore the original implementations of these  
5 algorithms were used.

6

## 7 **3 Data and methods**

### 8 **3.1 Input data**

9 Single swath Tbs were used as input to the algorithms. The SMMR data were obtained from  
10 the US National Snow and Ice Data Centre – NSIDC (25 October 1978 to 20 August 1987,  
11 Njoku, 2003), EUMETSAT CM-SAF provided the SSM/I data (covering 9 July 1987 to 31  
12 December 2008, Fennig et al., 2013), and AMSR-E data were from NSIDC (from 19 June  
13 2002 to 3 October 2011; Ashcroft and Wentz, 2003). The footprints of all the channels were  
14 matched and projected onto following footprints: the 6 GHz footprint of 75 km × 43 km for  
15 AMSR; SSM/I and SMMR channels were averaged to approximately 75 km x 75 km areas  
16 for all channels, except 6 GHz and 10 GHz of SMMR, which were used in their original  
17 resolution of 148 km × 95 km and 91 km × 59 km respectively.

18 It is important to note that different datasets may have different calibration, and it can even be  
19 the case for different versions of the same dataset. Therefore the results presented in the  
20 following (especially the derived tie points) should be applied to other datasets with caution.

### 21 **3.2 Validation data**

22 Ideally, every algorithm should be evaluated over open water, at intermediate concentrations  
23 and over 100% ice cover. In practise, it is difficult to find high quality reference data at  
24 intermediate concentrations, especially for large areas covering entire satellite footprint (e.g.,  
25 70 km × 45 km for SSM/I at 19.3 GHz) and covering all seasons and ice types. Since the  
26 relationship between SIC and Tbs at all frequencies is assumed linear (except for the various  
27 noise contributions and a slight nonlinearity of the ASI algorithm), we argue that errors at  
28 intermediate concentrations can be found by linear interpolation between errors at 0% and  
29 100%. Thus the RRDP was built for validation of the algorithms at 0% and 100% SIC.

1 For the Open Water (OW) validation dataset (SIC = 0%), areas of open water were found  
2 using ice charts from Danish Meteorological Institute (DMI) and the US National Ice Center  
3 (NIC). The validation dataset for 0% SIC covered the following time periods: 1978-1987  
4 (SMMR), 1987-2008 (SSM/I), and 2002-2011 (AMSR-E). For this paper we used the subsets  
5 of 1978-1985 for SMMR, 1988-2008 for SSM/I and the full AMSR-E dataset.

6 To create the Closed Ice (CI) validation dataset (SIC = 100%), areas of convergence were  
7 identified in ENVISAT ASAR (Advanced SAR) derived sea ice drift fields available from the  
8 PolarView (<http://www.polarview.org>) and MyOcean (<http://www.myocean.eu>) projects. The  
9 basic assumption for the convergence method to provide 100% sea ice is that during winter  
10 after 24 hours of net convergence the open water areas (leads) have either closed or refroze.  
11 During summer this assumption does not hold due to the presence of melt ponds and the lack  
12 of refreezing. The CI dataset is therefore only valid for accurate tests during winter (October–  
13 April in the Northern Hemisphere and May–September in the Southern Hemisphere). The CI  
14 dataset covered years 2007-2008 for SSM/I and 2007-2011 for AMSR-E. SMMR was not  
15 included, because there were no SAR data available at that time. Note that the CI reference  
16 dataset may still have some small fraction of residual open water. This however, does not  
17 jeopardize our use of the minimum standard deviation as a measure of algorithm performance,  
18 since we are only looking for the relative differences between algorithms.

19 Fig. 1 (Northern Hemisphere) and Fig. 2 (Southern Hemisphere) show the coverage of a  
20 subset of the RRDP for the SSM/I instrument during winters of 2007 and 2008, which  
21 contains about 30,000 data points. The dataset also includes the areas where there normally  
22 should not be any ice (blue triangles in the left panels of the figures) in order to test the ability  
23 of the algorithms to capture these correctly. The coverage of the RRDP is displayed both in  
24 terms of Tbs in the 6 channels of the SSM/I instrument (main panels), and spatial distribution  
25 (embedded maps). The other years, mentioned above and not shown in the figures, include  
26 approximately 4,000 data points per year, except the SMMR period with about 1,000 points  
27 per year, but the full dataset extends from 1978 to 2011. We are confident that these locations  
28 represent the full amplitude of weather influence on measured Tbs and hence retrieved  
29 SICs. The left panels of Fig. 1 and Fig. 2 show the RRDP SSM/I subset in a classic (Tb37v,  
30 Tb19v)-space, which is the one sustaining the BF algorithm (or CV). The ice line extends  
31 along different ice types. In the Northern Hemisphere, ice types vary from MYI with lower  
32 values of Tb37h (colouring) to first-year ice (FYI) with higher values of Tb37h. In the

1 Southern Hemisphere, the ice line extends between ice types A, representing FYI, and B, sea  
2 ice with a heavy snow cover (Gloersen et al., 1992). The so-called FYI and MYI tie points  
3 would typically lie along this line. The location of these different ice types can be seen on the  
4 embedded maps, and matches the expected distribution of older and younger ice in the  
5 Northern Hemisphere. In the (Tb37v, Tb19v)-space, the OW symbols are grouped mostly in  
6 one point (OW tie point), but also present some spread due to the noise induced by  
7 geophysical parameters such as atmospheric water vapour, liquid water- and ice clouds,  
8 surface temperature variability and surface roughening by wind (all collectively called  
9 geophysical noise). Note that the majority of the symbols is grouped around one point and a  
10 lot less are spread along the line, however this is not easy to see from the plots because many  
11 points are hidden behind each other. The Tb22v colouring of the OW symbols illustrates how  
12 the variability of the OW signature is mostly driven by factors impacting also the 22 GHz  
13 channel (atmospheric water vapour content). The length and orientation of the OW spread,  
14 and especially the distance from the OW points to the line of ice points, determines the  
15 strength of algorithms built on these frequencies (e.g. BF or CV) at low SIC.

16 The right panels show the same areas but in a (Tb85v, Tb85h)-space. The ice line is very well  
17 defined (limited lateral spread), almost with a slope of one. However, it is difficult to define  
18 an OW point in this axis, since samples are now spread along a line. This “weather line” even  
19 intersects the ice line, illustrating that algorithms based purely in the (Tb85v, Tb85h)-space  
20 (like the ASI and N90 algorithms) have difficulties at discriminating open water from sea ice  
21 under certain atmospheric conditions (Kern, 2004).

22 The embedded maps display the winter location of the OW samples (same location for the  
23 whole RRDP, for all instruments). In both hemispheres, these locations follow sea ice retreat  
24 in summer months to always capture ocean/atmosphere conditions in the vicinity of sea ice  
25 (not shown). The absence of data near the North Pole is due to the ENVISAT ASAR not  
26 covering areas north of 87°. The somewhat limited coverage of the sea ice samples of the  
27 Pacific sector in the Northern Hemisphere and many areas in the Southern Hemisphere is due  
28 to scene acquisition strategies of the ENVISAT mission.

29 After validation of the algorithms using the obtained datasets at 0% and 100% we found that  
30 some of the algorithms are hard to validate at these values because they are not designed to  
31 enable retrievals outside the SIC range of 0% –100% (NASA Team2, ECICE) or are affected  
32 by a combination of large bias and nonlinearity at high SIC (ASI). This complicates

1 comparison of these algorithms directly to other algorithms because these effects cut part of  
2 SD of the retrieved SIC, while we aim at evaluating the full variability around these reference  
3 values (0% and 100%). We implemented the algorithms (except these three) without cut-offs,  
4 allowing thus SIC values below 0% and above 100% as well. In order to be able to include  
5 these three algorithms in the inter-comparison, we have produced reference datasets of Tbs in  
6 every channel that correspond to values of SIC 15% and 75% for an additional evaluation. We  
7 find that the algorithms' performance at 15% is representative of that at 0%, and so is 75% to  
8 100%. Therefore we show the results of evaluation only at SIC 15% and 75%. By  
9 "representative" here we mean that the algorithms' ranking does not change significantly  
10 (more details in Sect. 4.1. and Table 2) even though the absolute values of SD are different.

11 The SIC 15% dataset was constructed by mixing the average FYI signature (Tb) with the OW  
12 dataset, i.e.

$$13 \quad Tb_{15} = 0.85 * Tb_0(t) + 0.15 * Tb_{100}(\overline{FY}), \quad (1)$$

14 where Tb<sub>0</sub> (OW Tb) is multiplied by 0.85 (85% water) and is varying with time, while Tb<sub>100</sub>  
15 (ICE Tb) is multiplied by 0.15 (15% ice) and is an average value of the FYI signature  
16 constant for all data points from the RRDP (see above) for a given year. By using the SIC  
17 15% dataset we aim at testing sensitivity of the algorithms to the atmospheric influence over  
18 the ocean and not to variability in emissivity of ice. Therefore we keep Tb of ice constant.

19 The SIC 75% dataset was generated similarly to the SIC 15% dataset, but with full variability  
20 of ice and 25% of the average OW signature:

$$21 \quad Tb_{75} = 0.75 * Tb_{100}(t) + 0.25 * Tb_0(\overline{OW}). \quad (2)$$

22 For the SIC 75% dataset the variability in Tbs is driven by variability at SIC 100%  
23 (Tb<sub>100</sub>(t)), and not at SIC 0%. We keep SIC 0% Tb (Tb<sub>0</sub>) constant at the average value of the  
24 OW signature for a given year in order to avoid the influence of seasonally varying  
25 atmospheric conditions, which would have happened if we mixed variable SIC 100% Tbs  
26 with variable SIC 0% Tbs. As a consequence, the SIC 75% dataset will reflect a lower  
27 atmospheric variability than we would have to expect from a real SIC 75% dataset. Since the  
28 CI dataset is only valid for the winter season, the same applies for this SIC 75% dataset.

29 It is noteworthy that we originally had designed a reference dataset of SIC 85%, but the  
30 positive biases of the ASI and NASA Team 2 algorithms were larger than 15% and thus part  
31 of the SD was still cut-off at 100%. Therefore it was necessary to use a SIC 75% dataset

1 instead. The performance of the algorithms was consistent between the SIC 75%, 85% and  
2 100% datasets, and therefore we consider such substitution acceptable. This way of mixing  
3 Tbs is not entirely physical since we are mixing Tbs seen through two different atmospheres.  
4 However, since the majority of the signal originates from either open water or ice, and we use  
5 fixed Tbs for the remaining fraction, we consider the results to be still reasonably  
6 representative for algorithm performance evaluation.

7 Normally, SIC products are truncated at 0% and 100% to allow only physically meaningful  
8 SIC values, though this does not apply to ECICE because it employs the inequality constraint  
9 of  $0\% < SIC < 100\%$  in its optimization formulation. However, as the intention here is to  
10 investigate the statistical properties of the retrievals, we will analyse actual SIC as retrieved  
11 with the algorithms, without truncation, which means the retrieved values can be negative or  
12 above 100%. Instrument and geophysical noise cause the Tbs to vary around the chosen tie  
13 points, and it cannot be avoided that at least a part of this noise is translated into some noise in  
14 the retrieved SIC.

### 15 **3.3 Reference dataset for melt pond sensitivity assessment**

16 Daily gridded SIC and melt pond fraction (MPF) reference dataset for the Arctic (Rösel et al.,  
17 2012a) was derived from clear-sky measurements of reflectances in channels 1, 3 and 4 of the  
18 MODerate resolution Imaging Spectroradiometer (MODIS) in June–August 2009. The MPF  
19 is determined from classification based on a mixed-pixel approach. It is assumed that the  
20 reflectance measured over each MODIS  $500\text{ m} \times 500\text{ m}$  grid cell comprises contributions  
21 from three surface types: melt ponds, open water, sea ice/snow (Rösel et al., 2012a). By using  
22 known reflectance values (e.g. Tschudi et al., 2008) a neural network was built, trained, and  
23 applied (Rösel et al., 2012a). MPF is given as fraction of sea ice area (not grid cell) covered  
24 by melt ponds. For the sensitivity analysis in this work, a total of 8152 data points were  
25 selected from this dataset, so that SD of MPF over each  $100\text{ km} \times 100\text{ km}$  area was less than  
26 5%, SIC variations were less than 5%, SIC itself was larger than 95% and cloud cover less  
27 than 10%.

28 The MODIS data were undergone a bias correction (Mäkynen et al., 2014) based on an inter-  
29 comparison between ENVISAT ASAR wide swath mode (WSM) imagery, in-situ sea ice  
30 surface observations, weather station reports and the daily MODIS MPF and SIC dataset. It  
31 was found that the MODIS SIC was negatively biased by 3% and MPF was positively biased

1 by 8%. An investigation of the 8-day composite dataset of the MODIS MPF and SIC dataset  
2 with regard to their seasonal development during late spring/early summer confirmed the  
3 existence of such biases.

4 MODIS SIC was only used for the summer period to evaluate the algorithms performance  
5 over melt ponds, but not for the SIC validation. This is due to lack of a sufficiently quality-  
6 controlled MODIS SIC product with potential of a validation dataset. The cloud filters  
7 developed for lower latitudes are not reliable enough in the polar latitudes. Moreover,  
8 identification of ice/water in the images depends on thresholds, which will bring the problem  
9 of tie points. The validation of the MPF dataset by Rösel et al. (2012a) revealed accuracy of  
10 5% to 10%. Because of the methodology used, the MPF is tied to the other two surface types:  
11 open water in leads and openings between the ice floes and sea ice / snow. Therefore it can be  
12 assumed that the accuracy of the fraction of these two other surface types is of the same  
13 magnitude as that of the MPF: 5% to 10%, which can be considered as not sufficient for  
14 quantitative SIC evaluation.

#### 15 **3.4 Reference dataset for the thin ice tests**

16 Sensitivity of the algorithms to thickness of thin ( $\leq 50$  cm) sea ice was evaluated using a thin  
17 ice thickness dataset for the Arctic Ocean, compiled for this particular purpose. To produce  
18 this dataset, large (100 km diameter) homogenous areas of  $\sim 100\%$  thin ice were identified as  
19 areas with dark and homogenous texture by visual inspection of 175 ENVISAT ASAR WSM  
20 scenes. The same procedure as when producing ice charts was applied. Thin ice thickness was  
21 subsequently derived for these areas using ESA's L-band Soil Moisture and Ocean Salinity  
22 (SMOS) observations (Huntemann et al., 2014; Heygster et al., 2014). The dataset covers the  
23 time period from 1 October to 12 December 2010 and consists of 991 sea ice thickness data  
24 points. For these selected grid cells AMSR-E Tbs were extracted and used as input to the SIC  
25 algorithms.

#### 26 **3.5 Substitution of weather filters by atmospheric correction**

27 SIC retrievals can be contaminated due to wind roughening of the ocean surface, atmospheric  
28 water vapour and CLW, as well as precipitation. Traditionally, the atmospheric effects on the  
29 SIC retrievals are removed by applying an open water/weather filter based on gradient ratios  
30 of Tbs for SMMR (Gloersen and Cavalieri, 1986) and SSM/I (Cavalieri et al., 1995):

$$1 \quad \quad \quad SMMR: SIC = 0 \quad \text{if } GR(18/37) > 0.07 \quad (3)$$

$$2 \quad \quad \quad SSM/I: SIC = 0 \quad \text{if } GR(19/37) > 0.05 \text{ and/or } GR(19/22) > 0.045, \quad (4)$$

3 where the gradient ratios of Tb18v (Tb19v) and Tb37v ( $GR(18/37)$  and  $GR(19/37)$ ) are most  
4 sensitive to CLW and the gradient ratio of Tb19v and Tb22v ( $GR(19/22)$ ) mainly detects  
5 water vapour. We tested the performance of this technique (more details in Sect. 4.4), and  
6 found that it is removing not only atmospheric effects but also ice itself, which we found to be  
7 unacceptable for a SIC algorithm.

8 Therefore we chose not to use the open water/weather filters, but implement an alternative  
9 solution, following Andersen et al. (2006) and Kern (2004). The suggested method consists of  
10 applying a more direct atmospheric correction methodology, where the input SSM/I Tbs in all  
11 the channels used by the algorithms are corrected with regard to atmospheric and surface  
12 effects using a Radiative Transfer Model (RTM):

$$13 \quad \quad \quad Tb_{corr} = Tb_{measured} - (Tb_{atm} - Tb_{ref}) \quad (5)$$

$$14 \quad \quad \quad Tb_{atm} = Tb(f, p, WS, WV, CLW, SST, T_{ice}, SIC, FMYI) \quad (6)$$

$$15 \quad \quad \quad Tb_{ref} = Tb(f, p, 0, 0, 0, SST_{ref}, T_{ice\ ref}, SIC, FMYI), \quad (7)$$

16 where f – frequency, p – polarisation, WS – wind speed, WV – water vapour, SST – sea  
17 surface temperature,  $T_{ice}$  – ice temperature, and FMYI – MYI fraction (Meissner and Wentz,  
18 2012 and Wentz, 1997).  $Tb_{corr}$  is measured Tb minus the difference between simulations  
19 with ( $Tb_{atm}$ ) and without ( $Tb_{ref}$ ) atmospheric effects (Meissner and Wentz, 2012 and Wentz,  
20 1997). In order to calculate  $Tb_{ref}$ , zero values were assigned to WS, WV and CLW, while  
21  $SST_{ref} = 271.5K$  and  $T_{ice\ ref} = 265K$ . 3-hourly fields of 10 m wind speed, total columnar  
22 water vapour, and 2 m air temperature from the ECMWF ERA-Interim Numerical Weather  
23 Prediction (NWP) re-analysis were used in this process. Following the results of Andersen et  
24 al. (2006) we did not use CLW and precipitation from the NWP data because these are  
25 considered to be less consistent with the observed Tbs (also confirmed by our own analysis).  
26 Therefore CLW is 0 also when calculating  $Tb_{atm}$  in this case. The NWP model grid cells are  
27 collocated with the AMSR-E/SSM/I swath Tbs in time and space. Using the 3-hourly NWP  
28 fields we ensure a time difference between the NWP data and the satellite data to be within  
29 1.5 h.

1 In order to evaluate the effect of suggested atmospheric correction for SSM/I we selected six  
2 test sites in the Arctic, which are subject to different weather types: for some it is more  
3 common to have storms and strong winds, and some are typically quieter. The total amount of  
4 points sampled at these locations is 2320 and covers the entire year 2008. The results obtained  
5 were similar for AMSR-E (not shown here).

### 6 **3.6 The validation/evaluation procedure**

7 Tbs from the three microwave radiometer instruments (AMSR-E, SSM/I and SMMR, Sect.  
8 3.1) were extracted and collocated with the reference datasets introduced above for open  
9 water, closed ice, melt ponds, and thin ice in the RRDP. These Tb data were then used as  
10 input to the SIC algorithms.

11 The criteria for the validation and evaluation procedure were aimed at minimizing the  
12 sensitivity to the atmospheric effects and surface emissivity variations as described in the  
13 Introduction. In addition, we considered the following aspects: 1) data record length:  
14 algorithms using near 90 GHz channels cannot be used before 1991 when the first functional  
15 SSM/I 85 GHz radiometer started to provide consistent data, 2) spatial resolution: ranges from  
16 over 100 km to less than 10 km for different channels and instruments, 3) performance along  
17 the ice edge, where new ice formation is common in winter, and 4) performance during the  
18 summer melt. Additional criteria for the algorithm selection were: the possibility of reducing  
19 regional error using, e.g., NWP data and forward models; and the possibility to use dynamic  
20 tie points. The latter is to reduce sensitivity to inter-sensor calibration differences and error  
21 sources, which may be characterized by seasonal and inter-annual variability and/or have  
22 global and regional climatological trends.

23

## 24 **4 Results**

### 25 **4.1 The SIC algorithms inter-comparison and evaluation**

26 To evaluate performance of the algorithms, SD (Table 2) and bias (not shown) relative to the  
27 validation datasets (Sect. 3.2) were calculated for summer and winter separately. The  
28 algorithms in the Table 2 are sorted by the average SD of all the cases, starting with the  
29 smallest one. These values are averages weighted by the number of years when data were  
30 available for each instrument, thus giving more weight to SSM/I as the one providing the

1 longest dataset. SSM/I data were available during 21 years (1988–2008) for the low-  
2 frequency algorithms, i.e. the algorithms using frequencies up to 37 GHz (except 6H because  
3 this channel was not available on SSM/I), and for high-frequency algorithms during 17 years  
4 (1992–2008). SMMR did not have high frequencies and thus only applies to the low-  
5 frequency algorithms (8.7 years, November 1978–1987). The reference column (Ref) in the  
6 Table 2 contains SD of the full SIC 0% and SIC 100% datasets. It shows that the SD of the  
7 algorithms relative to each other, that is the algorithms ranking, does not change significantly  
8 when substituting SIC 100% dataset with SIC 75%, and SIC 0% dataset with SIC 15%.  
9 However, the absolute values of SD are altered.

10 The high-frequency algorithms ASI and N90 have a clear difference in SDs at low and high  
11 SIC. This is also true for the CV+N90 algorithm, but the separation is smaller as this hybrid  
12 algorithm also contains a low-frequency component. The large SDs for these algorithms  
13 mainly originate from the low SIC cases, where the atmospheric influence is more  
14 pronounced than it is for the low-frequency algorithms. Winter SDs for most of the  
15 algorithms tend to be lower than the ones of summer in the same category of SIC and  
16 instrument.

17 We chose to not show the biases here because we put more weight on SD in the algorithm  
18 evaluation. The bias was found to be similar within low- and high-frequency algorithm  
19 categories and it was sensitive to the choice of tie points, which made it less suitable for the  
20 evaluation procedure. In the Northern Hemisphere the stronger negative biases were  
21 dominated by the high SIC cases (with the exception of the N90, CV+N90, NT2 and ASI),  
22 while stronger positive biases were dominated by the low SIC cases. Algorithms ASI, NT2  
23 and ECICE were positively biased for all the cases in both hemispheres. Note that the  
24 algorithms ECICE and ASI were developed for the Northern Hemisphere, but were applied to  
25 both hemispheres in this study. These three algorithms are the only ones for which it was not  
26 possible to use the RRDP tie points as was done for the other algorithms, and this may explain  
27 part of the bias (see Sect. 4.5 for further discussion on tie points). For the algorithms with  
28 large biases and cut-offs at SIC 100%, the bias reduces our ability to estimate their SD  
29 properly using the chosen approach and thus makes them look better than they really are at  
30 high SIC (>75%). For example, if real SIC is 75%, an algorithm with a positive bias of 20%  
31 will have average SIC of 95%, and by cutting-off all the values above 100% it reduces the

1 scatter, and thus SD, to only the values in 95-100% interval. In contrast, for an algorithm with  
2 same bias and no cut-off the full scatter will be preserved and represented by a higher SD.

3 At SIC 15% the CV (BF) algorithm had the second lowest SD (3.8% in the Northern  
4 Hemisphere and 3.5% in the Southern Hemisphere) after the 6H algorithm. Even though the  
5 6H showed such a low SD, we did not consider it as a suitable algorithm for a climate dataset  
6 because this algorithm could not be applied to SSM/I data, which shortens the time series  
7 significantly. At SIC 75% the BR algorithm had the lowest SD of 3.1% in the Northern  
8 Hemisphere and 2.9% in the Southern Hemisphere.

9 Difference in SD between summer and winter (only SIC 15%) was lowest for the algorithms  
10 NT, NT+CV, BR, CV and OSISAF (average over both hemispheres and all three instruments  
11 amounted to 0.2–0.3%). The algorithms ESMR, ECICE, 6H, NT2 and CV+N90 had higher  
12 summer-winter differences (0.4–0.5%), while the remaining algorithms (BP, N90 and ASI)  
13 showed the highest values of 0.8–1.2%.

## 14 **4.2 Melt Ponds**

15 The SIC and MPF from MODIS were collocated with daily SIC retrieved by the algorithms in  
16 the Arctic Ocean for June–August 2009 to investigate the sensitivity of the algorithms to melt  
17 ponds. Due to the low penetration depth, we expect that passive microwave SIC algorithms  
18 interpret melt ponds as open water and hence in summer they provide the net ice surface  
19 fraction ( $C$ ), which excludes leads and melt ponds, rather than traditional SIC. Therefore we  
20 compute corresponding parameter from the MODIS data:

$$21 \quad C = (1 - W) = SIC_{MODIS} - SIC_{MODIS} * MPF, \quad (8)$$

22 where  $W$  is surface fraction of water (leads + melt ponds). Fig. 3 shows SIC calculated by  
23 four selected SIC algorithms (CV, BR, N90 and NT) as a function of  $C$ . Note that because of  
24 the limitation to MSIC > 95% the variation in the net ice surface fraction is almost solely due  
25 to the variation in MPF, which was varying from 0 to 50% for the selected dataset.

26 There is a pronounced overestimation of the net ice surface fraction by the CV and BR  
27 algorithms that compose the OSISAF combination (however only BR is used for high SIC).  
28 For example, at  $C = 90\%$  the average SIC is 128% (CV), 115% (BR), 103% (N90) and 100%  
29 (NT). The slopes of the regression lines are close to one (0.9–1.2 for the shown algorithms),  
30 which agrees with the assumption that melt ponds are interpreted as open water by microwave

1 radiometry. The NT algorithm shows SIC values closest to C (the least bias of the four  
2 algorithms), which adds to our argument for using this algorithm for defining areas of high  
3 SIC (NT > 95%) for retrieval of the dynamic tie points (Sect. 4.5).

#### 4 **4.3 Thin ice**

5 Sensitivity of selected SIC algorithms (CV, BR, OSISAF, N90, NT and 6H) to thin sea ice  
6 thickness was investigated. Fig. 4 shows SIC obtained by these algorithms as a function of sea  
7 ice thickness from SMOS (Sect. 3.4). The data are shown as averages for each sea ice  
8 thickness bin of 5 cm width with the number of measurements in each bin shown on the  
9 figure (total number of measurements is 991). The grey shading shows SD, which is  
10 calculated from all the SIC retrievals in the given bin. These SDs are calculated for each  
11 algorithm individually, but overlap each other on the figure. Since in the OSISAF  
12 combination the BR algorithm has weight of 1 for high SIC, these algorithms show identical  
13 results; therefore BR is not visible.

14 The SIC is known to be ~100% for the cases selected, therefore one would expect all the  
15 curves to be horizontal and placed at high SIC. However, this is not going to be the case  
16 following published knowledge suggesting that SIC is underestimated for thin ice (Kwok et  
17 al., 2007, Grenfell et al., 1992). Hence, we are interested in the point where a given algorithm  
18 is no longer affected by the ice thickness. All the algorithms underestimate the SIC for ice  
19 thickness of up to 25 cm. Note that most of the algorithms also show a negative bias of about  
20 5% for ice thickness above 30 cm, i.e. ice which is not termed thin ice anymore. This could be  
21 caused by the fact that the thin ice identified in SAR images is on average smoother/less  
22 deformed and most likely has less snow than the ice used for the derivation of the sea ice tie  
23 points applied in the algorithms.

24 Out of the five algorithms shown, N90 levels off, that is the SIC value varies by less than 5%  
25 between the neighbouring bins of SIT, at the lowest thicknesses (20–25 cm). The OSISAF  
26 and CV follow at the thicknesses of 25–30 cm, and NT and 6H at 30–35 cm. The slightly  
27 better performance of CV relative to OSISAF suggests a shift in the mixing of BR and CV in  
28 a new algorithm (using CV at higher intermediate concentrations); see the introduction of the  
29 SICCI algorithm in the discussion section. More details on the algorithm's performance over  
30 thin ice can be found in Heygster et al. (2014).

#### 1 **4.4 Atmospheric correction**

2 First we implemented traditional open water/weather filters (Eqs. 3 and 4), which work as ice-  
3 water classifiers. These filters set pixels to SIC 0% when they are classified as ones subjected  
4 to a high atmospheric influence over open water. This efficiently removes noise due to the  
5 weather influence in open water regions.

6 However, we found, as did also Andersen et al. (2006), that open water/weather filters also  
7 eliminate low concentration ice (up to 30%). This is illustrated in Fig. 5, where intermediate  
8 concentration datasets were generated using equations similar to Eq. (1) from the same Tbs as  
9 used for the algorithms inter-comparison (Sect. 4.1). The filter identifies correctly the pixels,  
10 which do not contain any ice (SIC = 0%): practically all pixels are located outside the red  
11 square in the upper left plot. The filter keeps almost all the pixels containing sea ice (SIC =  
12 30%): almost all pixels are located inside the red square in the bottom right plot; only a  
13 handful values fall outside the range defined by the red box and is set to 0%. However for the  
14 cases of SIC 15% and 20%, which are shown here as an example, the filter sets SIC to 0% for  
15 all the pixels outside the red square in the upper right and bottom left plots, which  
16 corresponds to 27% of the total amount of pixels (3320) for the SIC 15% and to 9% for the  
17 SIC 20%.

18 In order to avoid this truncation of real SIC by the open water/weather filter, we investigated  
19 an alternative approach where we applied atmospheric correction to the Tbs, as described in  
20 Sect. 3.5, before using them as input to the algorithms. The correction reduced the Tb  
21 variance by 22–35 % (19 GHz and 37 GHz channels) and up to 40% (near 90 GHz channels)  
22 when water vapour, wind speed and 2 m temperature were used in the correction scheme.  
23 Adding CLW as the fourth parameter worsened the results (19 GHz and 37 GHz channels).  
24 CLW has high spatial and temporal variability and the current ERA Interim resolution and  
25 performance for CLW is not suitable for this correction. In the following the satellite data are  
26 therefore not corrected for the influence of CLW.

27 To illustrate the effect of the correction, we compared the SD of SIC computed from Tbs with  
28 and without correction for water vapour, wind speed and 2 m temperature (Fig. 6). The top  
29 plots show histograms of the SIC over open water for the OSISAF algorithm before the  
30 correction (left) and after (right). The distribution becomes clearly less noisy and tends to be  
31 more Gaussian-shaped. To show the effect of the correction on performance of all the  
32 algorithms (Table 1, except NT2 and ECICE), the SD of SIC is shown in the bottom plot. The

1 SD has decreased by 48–65% (of the original value) after the atmospheric correction for all  
2 the shown algorithms. The improvement due to the RTM correction shown in the Fig. 6 is an  
3 average measure for all the 2320 samples. It should be noted that the tie points need to be  
4 adjusted to the atmospherically corrected data. The tie points given in Appendix A are for  
5 uncorrected data.

#### 6 **4.5 Dynamic tie points**

7 As mentioned in the Introduction, not only sea ice area/extent is characterised by seasonal  
8 variability and has a trend, but so do also atmospheric and surface effects influencing the  
9 measured microwave emission. In order to compensate for these effects, we suggest that in an  
10 optimal approach tie points should be derived dynamically.

11 In order to generate dynamically adjusted daily tie points we first define the sampling areas  
12 for consolidated ice and open water at a distance of 100 km from the coasts. The area for the  
13 ice tie point is defined so that SIC is larger than 95% according to the NT algorithm and it is  
14 within the limits of maximum sea ice extent climatology (NSIDC, 1979–2007). The NT  
15 algorithm was chosen for this purpose because it is a standard relatively simple algorithm  
16 with little sensitivity to ice temperature variations (Cavalieri et al., 1984). The data for the  
17 open water tie point were selected geographically along two belts in the Northern and  
18 Southern hemispheres defined by the maximum sea ice extent climatology (200 km wide belt  
19 starting 150 km away from the climatology). Data points south of 50N were not used. Total of  
20 15,000 data points per day were selected.

21 Then 5,000 Tb measurements (every day) in these areas were randomly selected among the  
22 total of 15,000 data points and averaged using a 15-day running window ( $\pm 7$  days) to reduce  
23 potential noise in daily values. Selection of only 5,000 samples per day is to ensure that no  
24 days are weighted higher than others when there are differences in the number of data points  
25 from day to day. The 15-days window allows smoothing out the synoptic scales of weather  
26 perturbations and at the same time capture the onset of ice emissivity changes due to summer  
27 melt or fall freeze-up. We believe that longer time windows will induce additional (too much)  
28 smoothing over the ice, while shorter time-periods will introduce too much noise (over open  
29 water). The scatter of all the obtained 15,000 data points per day was used as a tie point  
30 uncertainty, which contributes to the total per-pixel daily uncertainty retrieved for SIC.

1 An example of ice tie point is presented in Fig. 7, top and middle panels, by Tb19v and Tb37v  
2 and in the bottom panels by slope of the ice line according to the Bootstrap scheme. We chose  
3 to not show the tie points of the Bristol algorithm because the polarization and frequency  
4 information from 19V, 37V and 37H channels is transformed into a 2D plane defined by x  
5 and y components (see Smith (1996) for more details), which are harder to relate to than Tbs.  
6 The open water tie points are not shown here as they have less seasonal variability (within 5  
7 K). The dynamic tie point for ice is represented by an average of the fraction of FYI and MYI  
8 in the samples of all ( $\pm 7days$ ) selected ice conditions ( $NT > 95\%$ ). Due to the change in the  
9 relative amount of FYI and MYI in the Arctic Ocean in recent years, the average ice tie point  
10 will move along the ice-line in the Tb space.

11 Fig. 7 demonstrates that the tie points are not constant values as it is assumed traditionally  
12 (static tie points from the RRDP, also averaged FYI and MYI values, are shown by horizontal  
13 lines), but rather geophysical parameters showing seasonal and inter-annual variations. This  
14 applies particularly to the melt season, which is highlighted by the grey vertical bars for three  
15 selected years in Fig. 7, bottom plots. Therefore the dynamic approach is more suitable for the  
16 SIC algorithms. The ice tie point may vary by about 30 K during one year, which amounts to  
17 approximately 8–10% of the average value. Sensor drift and inter-sensor differences are also  
18 important aspects, which might cause an unrealistic trend in the retrieved SIC when static tie  
19 points are applied. The dynamic tie point approach compensates for these effects.

20 A detailed description of the procedure to obtain dynamic tie points is given in the Appendix  
21 B. The tie points will vary with calibration of the input data/version number and source, so the  
22 tie points obtained here should not be used with other versions of the input data with potential  
23 different calibration. The procedure on the other hand can be applied to all  
24 versions/calibrations of the input data.

25

## 26 **5 Discussion**

### 27 **5.1 The SIC algorithms inter-comparison and evaluation**

28 Based on validation datasets of SIC 15% and 75% we used variability (SD) in the SIC  
29 produced by the different algorithms as a measure of the sensitivity to geophysical error  
30 sources and instrumental noise. The errors from geophysical sources over open water are  
31 generated by wind induced surface roughness, surface and atmospheric temperature

1 variability and atmospheric water vapour and CLW. Over ice, the errors are dominated by  
2 snow and ice emissivity and temperature variability, where parameters such as snow depth,  
3 and to some extent variability in snow density and ice emissivity are important (Tonboe and  
4 Andersen, 2004). The atmosphere plays only a minor role over ice except at near 90 GHz,  
5 where liquid water/ice clouds may still be a significant error source, especially in the  
6 Marginal Ice Zone. At the same time near 90 GHz data might be less sensitive to changes in  
7 physical properties in ice and snow because of the smaller penetration depth relative to the  
8 other frequencies used.

9 The algorithms 6H, CV, BR, OSISAF, NT and NT+CV, showed the lowest SDs (Table 2).  
10 The 6 GHz channel was not available on SSM/I, which provides the longest time series, and  
11 therefore the 6H algorithm was not considered to be an optimal SIC algorithm for a climate  
12 dataset. Bristol showed the lowest SD over high SIC (only winter is considered) while CV  
13 had the lowest SD for the low SIC cases, which suggests that combining these two algorithms  
14 would provide a good basis for an optimal SIC algorithm.

15 The differences in SDs between summer and winter are reflecting the sensitivity of different  
16 algorithms to wind, atmospheric humidity and other seasonally changing quantities. In  
17 addition, some of these quantities may have climatological trends. Therefore small difference  
18 between the summer and winter SDs is an asset for an algorithm. The algorithms NT,  
19 NT+CV, BR, CV and OSISAF showed the lowest summer-winter differences in SD (0.2–  
20 0.3% on average for both hemispheres and all three instruments).

21 Note that the two modes of the Bootstrap Algorithm in this study were tested separately. The  
22 frequency mode (BF) of the original algorithm is applied only when  $T_{b19v}$  is below the ice  
23 line minus 5 K (Comiso 1995), which is the case for both 15% and 75% case. Otherwise the  
24 polarisation mode (BP) should be applied. Thus, we did not show the tests of BP for what it is  
25 originally meant – SIC near 100%. This algorithm was still evaluated along with all the others  
26 for SIC 100%, and the test indicated that BP performed quite well, but BR showed somewhat  
27 lower SDs (by about 2%) and therefore was selected for the hybrid algorithm.

28 Evaluation of typical processing chain components, such as climatological masks, land  
29 contamination correction and gridding from swath to daily maps, is not covered by this study.  
30 This work is devoted to a systematic evaluation of algorithms using a limited but very  
31 accurate reference dataset (the RRDP). For the consistent evaluation exercise completed here,  
32 areas in the vicinity of land were excluded.

## 1 5.2 The SICCI algorithm

2 During the algorithm evaluation and inter-comparison exercise the SICCI algorithm was  
3 introduced. It is a slightly modified version of the OSISAF algorithm in order to achieve  
4 better performance over areas with thin ice. Similar to the OSISAF algorithm, it is constructed  
5 as a weighted combination of CV and BR algorithms. In order to take more advantage of the  
6 better performance of CV for thin ice, the weights are defined as follows. For SIC below  
7 70%, as obtained by CV, the weight of this algorithm is  $w_{CV} = 1$ , while for high values  
8 ( $\geq 90\%$ ) it is  $w_{CV} = 0$ . Different weights were tested on the thin ice dataset. The optimal  
9 values were chosen so that the hybrid algorithm performs better over thin ice, and at the same  
10 time keeps its performance in other conditions at the same level as the original OSISAF  
11 algorithm. For the values between 70% and 90% the weight for CV is defined as

$$12 \quad w_{CV} = 1 - \frac{SIC_{CV} - 0.7}{0.2}, \quad (9)$$

13 where  $SIC_{CV}$  is SIC (between 0 and 1) obtained by CV. The weight of BR is  $1 - w_{CV}$ . In the  
14 original OSISAF algorithm, values of 0% and 40% were used.

## 15 5.3 Melt ponds

16 Fig. 3 illustrates that the four algorithms shown (but this is also valid for all other algorithms)  
17 are sensitive to the MPF, which may mean that melt ponds are interpreted as open water by  
18 the algorithms. This is because microwave penetration into water is very small. Rösel et al.  
19 (2012b) showed that in areas with melt ponds SIC algorithms (ASI, NT2 and Bootstrap)  
20 underestimate SIC by up to 40% (corresponding to a MPF close to 40%). One may still argue  
21 that melt ponds should have different signature from that of open water due to the difference  
22 in their salinity. However, for such high frequencies as used in the algorithms (19 GHz and  
23 higher) and in cold water the salinity was found to play a less significant role (Meissner and  
24 Wentz, 2012; see also Ulaby et al., 1986). In addition, the footprint size is so large (e.g. 70 km  
25  $\times$  45 km for 19.3 GHz channel on SSM/I) that an unresolvable mixture of surfaces might be  
26 present in it.

27 For some applications it is important to interpret ponded ice as ice and not as open water.  
28 However, we believe that satellite microwave radiometry is incapable to estimate SIC  
29 correctly if a certain fraction of the sea ice is submerged under water. Therefore, we suggest  
30 accepting what microwave sensors actually can do; to estimate the net ice surface fraction.

1 The latter is similar to the well known SIC during most of the year until melt ponds have  
2 formed on top of the ice in the melting season. Additional data sources (for example MODIS)  
3 could be used to supplement summer retrievals of SIC. Unlike with microwave radiometry,  
4 open water in leads and openings between the ice floes can be discriminated from open water  
5 in melt ponds on ice floes by means of their different optical spectral properties.

6 The algorithms shown in Fig. 3 overestimate SIC, which can be caused by higher Tbs in the  
7 areas between melt ponds. During summer these areas comprise wet snow and/or bare ice  
8 with a different physical structure than during winter. Therefore these areas have radiometric  
9 properties potentially different from those of winter, when the RRDP ice tie points were  
10 developed. This is demonstrated by Fig. 7 where the grey bars highlight that seasonal changes  
11 in the dynamic tie points to be used in the SICCI algorithm vary particularly during the  
12 summer months. The comparison of passive microwave algorithms and MODIS SIC in Rösel  
13 et al. (2012b) showed that in the areas without melt ponds the passive microwave SIC was  
14 larger than that of MODIS. Note also, however, that the tie points used here differ from those  
15 in Rösel et al. (2012b). This complicates a quantitative comparison of their results with ours  
16 and, in turn, calls for such kind of systematic, consistent evaluation and inter-comparison as  
17 shown in the present paper. Using the dynamic tie points approach (Sect. 4.5) decreases this  
18 effect: the OSISAF algorithm on average overestimated SIC by 24% when fixed RRDP tie  
19 points were used (same as in the Fig. 3) and by 17% with dynamical tie points (this example  
20 is not shown in the figure). However, even with dynamic tie points, it is likely that the areas  
21 selected to derive the 100% ice tie point during summer contain melt ponds. If this would be  
22 the case and if the selected area would have an average melt pond fraction of 10%, then the  
23 100% ice tie point would not represent 100% ice but a net ice surface fraction of only 90%.  
24 When estimating dynamic tie points, an initial SIC estimate is needed. In our case this was  
25 done using pixels with NT SIC > 95%. This algorithm is less sensitive to the surface  
26 temperature variations because it is based on polarization and gradient ratios of Tbs, which  
27 more or less cancels out the physical temperature (Cavalieri et al. 1984). In addition, it is  
28 interpreting melt ponds as open water (Sect. 4.2). This means that using NT SIC > 95% we  
29 select areas with reasonably low MPF to determine the signature of ice, which helps to avoid  
30 introducing a bias to the tie points with measurements containing melt ponds.

## 1 **5.4 Thin ice**

2 All the algorithms shown for the thin ice test (Fig. 4) underestimate the SIC for ice  
3 thicknesses up to 35 cm, which confirms findings by others (see Introduction). The 6H  
4 algorithm showed the highest sensitivity to the sea ice thickness, which is in agreement with  
5 Scott et al. (2014) showing that Tbs at 6 GHz can be used to estimate thin ice thickness. The  
6 least sensitivity to thickness of thin ice was observed for the N90 algorithm; the SIC obtained  
7 by this algorithm was independent of SIT values already at thicknesses of 20–25 cm. This is  
8 caused most likely by a smaller penetration depth in the near 90 GHz channels (shorter wave  
9 length) (see also Grenfell et al., 1998). OSISAF and CV had the second least sensitivity  
10 (levelled off at 25–30 cm), which adds more weight to the choice of an OSISAF-like  
11 combination as an optimal algorithm. We suggest that, when areas of thin ice are interpreted  
12 as reduced concentration, this should be clearly stated along with an eventual SIC product.  
13 This issue is similar to melt ponds in a way that there is no simple solution, and one should be  
14 aware of the limitation, which we demonstrate by the Fig. 4. In this study we manage to  
15 quantify the effect and thus allow modellers to assimilate SIC data in a more proper way.  
16 Implementation of an algorithm that accounts for thin ice (Röhrs and Kaleschke, 2012; Röhrs  
17 et al., 2012; Naoki et al., 2008; Grenfell et al., 1992) as an additional module to this optimal  
18 algorithm could be a potential improvement. For shorter datasets, a thin ice detection  
19 technique developed for AMSR-E and SSMIS (Mäkynen and Similä, 2015) can be  
20 incorporated in order to provide a thin-ice flag.

## 21 **5.5 Atmospheric correction**

22 Using the RTM of Wentz (1997), we concluded that over open water, most of the algorithms  
23 were sensitive to CLW although the sensitivities of CV and 6H were small (not shown).  
24 However, we found that CLW and precipitation are less reliable in ERA Interim data and  
25 therefore represent error sources, which we cannot correct for using the suggested method.  
26 This is also confirmed in literature (Andersen et al., 2006). Therefore, it is important to select  
27 a less sensitive algorithm (e.g., CV). The algorithms BP, ASI and N90 were very sensitive to  
28 this component (not shown). Most of the algorithms were sensitive to water vapour over open  
29 water, especially BP, ASI and N90. Some of the algorithms show some sensitivity to wind  
30 (ocean surface roughness), e.g. NT and BR. But we corrected for the water vapour and wind  
31 roughening by applying the RTM correction (see Fig. 6).

1 It was found that atmospheric correction of  $T_b$ s for wind speed, water vapour and temperature  
2 reduces the SD in retrieved SIC for all tested algorithms at low SIC. In addition, the shape of  
3 SIC distribution got closer to Gaussian after the correction (Fig. 6). The OSISAF combination  
4 (19V/37V) improved significantly after correction over open water. Over ice the atmospheric  
5 influence is small, as was shown by the ERA Interim data we used - total water vapour and  
6 CLW content over ice were much smaller than over ocean. The atmosphere over ice is  
7 generally much colder than over ocean, and cold air can contain much less moisture  
8 (including clouds) than warmer air. In addition, when the emissivity is much larger over sea  
9 ice (e.g. FYI) than open water, a change in the atmospheric water vapour imposes a smaller  
10 change in the  $T_b$  measured over sea ice compared to the one measured over open water  
11 (Oelke, 1997). Correction for the effect of surface temperature variations at SIC 100%, where  
12 2 m temperature was used as a proxy, was not effective. This can be explained by the fact that  
13 different wavelengths penetrate to different depth in the ice and thus should retrieve different  
14 temperatures.

15 The limitation of the applied correction is that, even though it reduces the atmospheric noise  
16 considerably, it does not remove it completely. There will therefore be some residual  
17 atmospheric noise over the ocean. We argue that this noise is more acceptable in a SIC  
18 algorithm than the removal of ice, but admit that this is debatable and for some applications  
19 the removal of ice may be preferable.

## 20 **5.6 Dynamic tie points**

21 The advantages of the suggested dynamical approach to retrieve tie points can be listed as  
22 follows. Firstly, it ensures long-term stability in sea ice climate record and decreases  
23 sensitivity to noise parameters with climatic trends. This is of importance because both sea ice  
24 area/extent and the geophysical noise parameters (sea ice emissivity, atmospheric parameters)  
25 have climatic trends. Also, as model study by Willmes et al. (2014) showed, emissivity of  
26 FYI covered by snow is characterized by seasonal and regional variations caused by  
27 atmospherically driven snow metamorphism. Secondly, the dynamical tie points are needed  
28 when accurately quantifying the SIC uncertainties. Thirdly, the dynamic tie point method in  
29 principle compensates for inter-sensor differences in a consistent manner, so no additional  
30 attempt was considered necessary to compensate explicitly for sensor drift or inter-sensor  
31 calibration differences (the SSM/I data have been inter-calibrated but not with the SMMR  
32 dataset).

1 The seasonal cycle in the tie points can be tracked across platforms (Fig. 7). Thus, the tie  
2 points are naturally changing geophysical parameters (or quantities obtained from such  
3 parameters), and should be dynamic as opposed to the traditional static approach. The  
4 variation amounts to approximately 20–30 K, which corresponds to about 8–12% of the  
5 average value, and the peaks in the variation occur in summer. Thus, increased variability in  
6 late spring/early summer connected to melt onset and consequent snow metamorphoses,  
7 reported by Willmes et al. (2014), is confirmed in our study.

8 The dynamic tie points approach is only applied in time, not in space. The aim of this study is  
9 to identify an optimal SIC algorithm for a climate dataset, which requires transparent  
10 description of techniques and uncertainties. It would be difficult to come up with proper  
11 uncertainty estimate in case we divide our region of interest - more or less arbitrarily - into  
12 sub-regions.

13 One might argue that different tie points for MYI and FYI can still be used. However,  
14 computation of the uncertainty at the boundary of both regions will become problematic. How  
15 shall one treat mixed pixels? And - most importantly - one would need a validated quality-  
16 controlled ice type dataset spanning the entire period. Therefore, we would recommend that  
17 regional (dynamic) tie points would be an ideal tool for regional applications and for near-real  
18 time SIC retrieval of spatially limited areas, but not for a climate dataset.

19

## 20 **6 Conclusions**

21 A SIC algorithm for climate time series should have low sensitivity to error sources,  
22 especially those that we cannot correct for (CLW and precipitation, see Sect. 5.5) and those,  
23 which may have climatic trends. When correcting for errors it is important to adjust the tie  
24 points in order to avoid introducing artificial trends from the auxiliary data sources (e.g. NWP  
25 data). Therefore the preferred algorithm should allow adjusting the tie points dynamically.  
26 The latter is necessary to compensate for climatic changes in the radiometric signature of ice  
27 and water; and eventual instrumental drift and inter-instrument bias. In addition, this  
28 algorithm should be accurate over the whole range of SIC from 0% to 100%. Along the ice  
29 edge spatial resolution and sensitivity to new ice and atmospheric effects is of particular  
30 concern. In order to produce a long climate data record, it is also important that the algorithm  
31 is based on a selection of channels for which the processing of long time-series is possible,

1 which are currently 19 GHz and 37 GHz. The comprehensive algorithm inter-comparison  
2 study reported here leads to following conclusions:

3 - The CalVal algorithm is among the best (low SD, Table 2a) of the simple algorithms at low  
4 SIC and over open water.

5 - The Bristol algorithm is the best (lowest SD, Table 2b) for high SIC.

6 - OSISAF-like combination of CalVal and Bristol is a good choice for an overall algorithm,  
7 using CalVal at low SIC and Bristol at high SIC.

8 In addition we conclude that:

9 - Melt ponds are interpreted as open water by all algorithms.

10 - Thin ice is seen as reduced SIC by all algorithms.

11 - After atmospheric correction of Tbs, low SIC become less uncertain (less noisy) than high  
12 SIC.

13 - Near 90 GHz algorithms are very sensitive to atmospheric effects at low SIC.

14 - All 10 algorithms shown in the Fig. 6 improve substantially when Tbs are corrected for  
15 atmospheric effects using RTM with NWP data. The additional 3 algorithms by nature could  
16 not be corrected/tested for this.

17 - The dynamic tie points approach can reduce systematic biases in SIC and alleviate the  
18 seasonal variability in SIC accuracy.

19 It is clear from these conclusions that there is no one single algorithm that is superior in all  
20 criteria, and it seems that a combination of algorithms (e.g., OSISAF or SICCI) is a good  
21 choice. An additional advantage of using a set of 19 GHz and 37 GHz algorithms is that the  
22 dataset extends from fall 1978 until today and into the foreseeable future.

23 Over ice the Bristol algorithm, chosen for the high SIC retrievals, is sensitive to the snow and  
24 ice temperature profile as well as to ice emissivity variations. Surface temperature is  
25 quantified in most NWP models, which means that there is a potential for correction. The  
26 Bristol algorithm performance over melting ice is good because the SIC as a function of net  
27 ice surface fraction has a slope close to one. The Bristol algorithm as other algorithms has a  
28 clear seasonal cycle in the apparent ice concentration at 100% SIC when using static tie

1 points. This means that dynamic tie points are an advantage when using Bristol (as with most  
2 of the other algorithms).

3 Over open water the CalVal algorithm, chosen for the low SIC retrievals, is among the  
4 algorithms with the lowest overall sensitivity to error sources including surface temperature,  
5 wind, and atmospheric water vapour. Importantly, the CalVal is relatively insensitive to  
6 CLW, which is a parameter we cannot correct for due to the uncertainty of this parameter in  
7 the NWP data at high latitudes. The response of CalVal to atmospheric correction gives a  
8 substantial reduction in the noise level. The response of CalVal to thin ice is better than that  
9 of the other 19 GHz and 37 GHz algorithms and comparable to near 90 GHz algorithms.

10 Therefore we suggest that an OSISAF or SICCI type of algorithm with dynamic tie points and  
11 atmospheric correction could be a good choice for SIC climate dataset retrievals. The  
12 selection of tie points should be done with careful attention to the melt pond issues in order to  
13 avoid melt pond contamination of the tie points in summer. Correction for wind speed, water  
14 vapour and surface temperature provides a clear noise reduction, but we found no  
15 improvement from correcting for NWP CLW.

16 In spite of their high resolution and good skill over ice, the near 90 GHz algorithms have  
17 some limitations for a SIC climate dataset because the near 90 GHz data were not available  
18 before 1991, and they are very sensitive to the atmospheric error sources over open water and  
19 near ice edge such as CLW. Finer spatial resolution achieved by the high-frequency channels  
20 does not offset the weather-induced SIC biases over open water and near ice edge. Model data  
21 used in the RTM to correct for the influence of surface wind speed, water vapor and air  
22 temperature have a coarser spatial resolution and hence will cause artifacts in the RTM-based  
23 correction. The remaining weather effects we cannot correct for (CLW and precipitation) will  
24 become even worse and more difficult to correct for because the model is even less capable to  
25 provide the information for this parameters at the same spatial scale as would be required.  
26 Their skill over ice is approximately the same as the one of the selected Bristol algorithm.

27 In the presented work we suggested a number of parameters, which could be used in order to  
28 select an optimal approach to retrieval of SIC climate dataset. We also suggested an approach  
29 that satisfies these requirements. However, we do not claim the suggested approach to be the  
30 best one taking into account that there is still a lot of potential for improvement in passive  
31 microwave methods.

32

1

2 **Appendix A: The RRDP tie points**

3 Table A1. The RRDP tie points: brightness temperatures in K

<b>Northern Hemisphere</b>									
	<b>AMSR-E</b>			<b>SSM/I</b>			<b>SMMR</b>		
	<b>OW</b>	<b>FYI</b>	<b>MYI</b>	<b>OW</b>	<b>FYI</b>	<b>MYI</b>	<b>OW</b>	<b>FYI</b>	<b>MYI</b>
<b>6V</b>	161.35	251.99	246.04				153.79	251.99	246.04
<b>6H</b>	82.13	232.08	221.19				86.49	232.08	221.19
<b>10V</b>	167.34	251.34	239.61				161.81	251.34	239.61
<b>10H</b>	88.26	234.01	216.31				95.59	234.01	216.31
<b>18V</b>	183.72	252.15	226.26	185.04	252.79	223.64	176.99	252.15	226.26
<b>18H</b>	108.46	237.54	207.78	117.16	238.20	206.46	111.45	237.54	207.78
<b>22V</b>	196.41	250.87	216.67	200.19	250.46	216.72	185.93	250.87	216.67
<b>22H</b>	128.23	236.72	199.60				135.98	236.72	199.60
<b>37V</b>	209.81	247.13	196.91	208.72	244.68	190.14	207.48	247.13	196.91
<b>37H</b>	145.29	235.01	184.94	149.39	233.25	179.68	147.67	235.01	184.94
<b>Near90V</b>	243.20	232.01	187.60	243.67	225.54	180.55			
<b>Near90H</b>	196.94	222.39	178.90	205.73	217.21	173.59			

<b>Southern Hemisphere</b>									
	<b>AMSR-E</b>			<b>SSM/I</b>			<b>SMMR</b>		
	<b>OW</b>	<b>FYI</b>	<b>MYI</b>	<b>OW</b>	<b>FYI</b>	<b>MYI</b>	<b>OW</b>	<b>FYI</b>	<b>MYI</b>
<b>6V</b>	159.69	257.04	254.18				148.60	257.04	254.18
<b>6H</b>	80.15	236.52	225.37				83.47	236.52	225.37
<b>10V</b>	166.31	257.23	251.65				159.12	257.23	251.65
<b>10H</b>	86.62	238.50	221.47				93.80	238.50	221.47

---

<b>18V</b>	185.34	258.58	246.10	185.02	259.92	246.27	175.39	258.58	246.10
<b>18H</b>	110.83	242.80	217.65	118.00	244.57	221.95	110.67	242.80	217.65
<b>22V</b>	201.53	257.56	240.65	198.66	257.85	242.01	186.10	257.56	240.65
<b>22H</b>	137.19	242.61	213.79				129.63	242.61	213.79
<b>37V</b>	212.57	253.84	226.51	209.59	254.39	226.46	207.57	253.84	226.51
<b>37H</b>	149.07	239.96	204.66	152.24	241.63	207.57	149.60	239.96	204.66
<b>Near90V</b>	247.59	242.81	210.22	242.41	244.84	211.98			
<b>Near90H</b>	207.20	232.40	197.78	206.12	235.76	200.88			

---

1

## 2 **Appendix B: Retrieval of the dynamic tie points**

3 Computing of the dynamic tie points involves two steps. First, a large number of  
4 characteristic Tb samples are selected for each day. Then, these data samples are aggregated  
5 over a temporal sliding window.

6 The open water tie point

7 The open water data samples are selected geographically within the limits of two 200 km  
8 wide belts, one in each hemisphere. Each belt follows the mask of maximum sea ice extent  
9 climatology, which was first extended 150 km away from the pole of the respective  
10 hemisphere. A land mask extending 100 km into open sea ensures that the open water  
11 signatures are not contaminated by land spill-over effects. In the Northern Hemisphere, data  
12 points south of 50N are discarded. A maximum of 5,000 randomly selected open water data  
13 samples are kept per day.

14 The daily open water tie point is computed as the average Tb of all selected open water data  
15 samples in a centred temporal sliding window ( $\pm 7$  days). The open water tie point is  
16 computed separately for each hemisphere.

17 The sea ice tie point

18 The sea ice data samples are selected geographically within maximum sea ice extent  
19 climatology for each hemisphere. The ice tie point data must in addition correspond to a SIC  
20 greater than 95%, as retrieved by the NASA Team algorithm using the tie points from the

1 Appendix A. Additional masks ensure that samples are taken away from the coastal regions.  
2 A maximum of 5,000 sea ice data samples are kept per day.

3 The daily sea ice tie point is computed over the same temporal sliding window as the open  
4 water tie point, and is computed separately for each hemisphere. The slope and offset of the  
5 ice line are computed using Principal Component Analysis. The ice line is the line in Tb space  
6 that goes through the FYI and MYI points (type-A and type-B ice in the Southern  
7 Hemisphere, see Fig. 1 and 2). Since the total SIC is our target (and not the partial  
8 concentrations of ice types), alternative versions of the CV and Bristol algorithms that rely on  
9 the slope and offset of the ice line were implemented. Additional criteria would be needed for  
10 further splitting the sea ice data samples into tie points based on ice types, this is not  
11 considered here.

12 A similar approach to deriving dynamic tie points is implemented for the sea ice  
13 concentration reprocessed dataset, and operational products of the EUMETSAT OSISAF.

14

## 15 **Acknowledgements**

16 This work was completed in the context of ESA Climate Change Initiative, Sea Ice project  
17 (SICCI) and was funded by ESA. The work of S. Kern was supported by the Center of  
18 Excellence for Climate System Analysis and Prediction (CliSAP). Support from the  
19 International Space Science Institute (ISSI), Bern, Switzerland, under project No. 245: Heil P.  
20 and S. Kern, ‘Towards an integrated retrieval of Antarctic sea ice volume’ is acknowledged.  
21 The EUMETSAT OSISAF (<http://osisaf.met.no>) granted access to an implementation of its  
22 SIC processing software, in particular the dynamic tie point retrieval process (see Appendix  
23 B).

24

## 25 **References**

26 Andersen, S., Tonboe, R., Kern, S., and Schyberg, H.: Improved retrieval of sea ice total  
27 concentration from spaceborne passive microwave observations using numerical weather  
28 prediction model fields: An intercomparison of nine algorithms, *Remote Sens. Environ.*, 104,  
29 374-392, 2006.

1 Andersen, S., Tonboe, R., Kaleschke, L., Heygster, G., and Pedersen, L. T.: Intercomparison  
2 of passive microwave sea ice concentration retrievals over the high-concentration Arctic sea  
3 ice, *J. Geophys. Res.*, 112, C08004, doi:10.1029/2006JC003543, 2007.

4 Ashcroft, P. and Wentz F. J.: AMSR-E/Aqua L2A Global Swath Spatially-Resampled  
5 Brightness Temperatures. Version 2., NASA DAAC at the National Snow and Ice Data  
6 Center, Boulder, Colorado USA, doi: 10.5067/AMSR-E/AE\_L2A.002, 2003.

7 Brucker, L., Cavalieri, D. J., Markus, T., and Ivanoff, A.: NASA Team 2 Sea Ice  
8 Concentration Algorithm Retrieval Uncertainty, *IEEE T. Geosci. Remote*, 52, 7336–7352,  
9 doi: [10.1109/TGRS.2014.2311376](https://doi.org/10.1109/TGRS.2014.2311376), 2014.

10 Cavalieri, D. J., Gloersen, P., and Campbell, W. J.: Determination of sea ice parameters with  
11 the NIMBUS 7 SMMR, *J. Geophys. Res.*, 89, D4, 5355–5369, 1984.

12 Cavalieri, D. J., Burns, B. A., and Onstott, R. G.: Investigation of the effects of summer melt  
13 on the calculation of sea ice concentration using active and passive microwave data, *J.*  
14 *Geophys. Res.*, 95, 5359–5369, 1990.

15 Cavalieri, D. J., Germain, K. S., and Swift, C. T.: Reduction of weather effects in the  
16 calculation of sea ice concentration with the DMSP SSM/I, *J. Glaciol.*, 41, 455-464, 1995.

17 Cavalieri, D. J. and Parkinson, C. L.: Arctic sea ice variability and trends, 1979–2010, *The*  
18 *Cryosphere*, 6, 881-889, doi:10.5194/tc-6-881-2012, 2012.

19 Comiso, J. C.: Characteristics of arctic winter sea ice from satellite multispectral microwave  
20 observations, *J. Geophys. Res.*, 91, 975–994, 1986.

21 Comiso, J. C.: SSM/I Sea Ice Concentrations Using the Bootstrap Algorithm, NASA  
22 Reference Publication 1380, NASA Center for Aerospace Information, 800 Elkridge Landing  
23 Road, Linthicum Heights, MD 21090-2934, (301) 62 1-0390, 1995.

24 Comiso, J. C. and Kwok, R.: Surface and radiative characteristics of the summer Arctic sea  
25 ice cover from multisensor satellite observations, *J. Geophys. Res.*, 101, 28397–28416, 1996.

26 Comiso, J. C.: Enhanced Sea Ice Concentrations and Ice Extents from AMSR-E Data, *J.*  
27 *Remote Sens. of Japan*, 29, 199–215, doi:10.11440/rssj.29.199, 2009.

28 Eastwood, S. (Ed.): Ocean & Sea Ice SAF (OSISAF) Sea Ice Product Manual. Version 3.8.,  
29 available at: <http://osisaf.met.no>, last access: May 2012.

1 Fennig, K., Andersson, A., and Schröder, M.: Fundamental Climate Data Record of SSM/I  
2 Brightness Temperatures, Satellite Application Facility on Climate Monitoring,  
3 doi:10.5676/EUM\_SAF\_CM/FCDR\_SSMI/V001, 2013.

4 Fetterer, F. and Untersteiner, N.: Observations of melt ponds on Arctic sea ice. *J. Geophys.*  
5 *Res.*, 103, 24821–24835, 1998.

6 Gloersen, P., and Cavalieri, D. J.: Reduction of Weather Effects in the Calculation of Sea Ice  
7 Concentration From Microwave Radiances, *J. Geophys. Res.*, 91, 3913–3919, 1986.

8 Gloersen, P., Campbell, W. J., Cavalieri, D. J., Comiso, J. C., Parkinson, C. L., and Zwally H.  
9 J.: Arctic and Antarctic Sea Ice, 1978–1987: satellite passive microwave observations and  
10 analysis, NASA SP-511, NASA, Washington, D.C., 1992.

11 Grenfell, T. C., Barber, D. G., Fung, A. K., Gow, A. J., Jezek, K. C., Knapp, E. J., Nghiem, S.  
12 V., Onstott, R. G., Perovich, D. K., Roesler, C. S., Swift, C. T., and Tanis, F.: Evolution of  
13 electromagnetic signatures of sea ice from initial formation to the establishment of thick first-  
14 year ice, *IEEE Trans. Geosci. Rem. Sens.*, 36(5), 1642-1654, 1998.

15 Grenfell, T. C., Cavalieri, D. J., Comiso, J. C., Drinkwater, M. R., Onstott, R. G., Rubinstein,  
16 I., Steffen, K., and Winebrenner, D. P.: Considerations for Microwave Remote Sensing of  
17 Thin Sea Ice, in: *Microwave Remote Sensing of Sea Ice* (ed F. D. Carsey), American  
18 Geophysical Union, Washington, D.C. doi: 10.1029/GM068p0291, 1992.

19 Heygster, G., Huntemann, M., Ivanova, N., Saldo, R., and Pedersen, L. T.: Response of  
20 passive microwave sea ice concentration algorithms to thin ice, *Proceedings Geoscience and*  
21 *Remote Sensing Symposium (IGARSS), 2014 IEEE International*, 13-18 July, Quebec City,  
22 QC, 3618 – 3621, doi:10.1109/IGARSS.2014.6947266, 2014.

23 Huntemann, M., Heygster, G., Kaleschke, L., Krumpen, T., Mäkynen, M., and Drusch, M.:  
24 Empirical sea ice thickness retrieval during the freeze up period from SMOS high incident  
25 angle observations, *The Cryosphere*, 8, 439-451, doi:10.5194/tc-8-439-2014, 2014.

26 Ivanova, N., Johannessen, O. M., Pedersen, L. T., and Tonboe, R. T.: Retrieval of Arctic Sea  
27 Ice Parameters by Satellite Passive Microwave Sensors: A Comparison of Eleven Sea Ice  
28 Algorithms, *IEEE T. Geosci. Remote*, 52, 7233–7246, doi:10.1109/TGRS.2014.2310136,  
29 2014.

1 Ivanova, N., Pedersen, L. T., and Tonboe, R., T.: Product Validation & Algorithm Selection  
2 Report (PVASR): Sea Ice Concentration, version 1.0, 20 June 2013, Doc Ref: SICCI-PVASR  
3 (SIC), European Space Agency, <http://esa-seaice-cci.org>, 2013.

4 Kaleschke, L., Lüpkes, C., Vihma, T., Haarpaintner, J., Bochert, A., Hartmann, J., and  
5 Heygster, G.: SSM/I Sea Ice Remote Sensing for Mesoscale Ocean-Atmosphere Interaction  
6 Analysis, *Can. J. Remote Sens.*, 27, 5, 526–537, 2001.

7 Kern, S.: A new method for medium-resolution sea ice analysis using weather-influence  
8 corrected Special Sensor Microwave/Imager 85 GHz data, *Int. J. Remote Sens.*, 25, 4555-  
9 4582, 2004.

10 Kern, S., Khvorostovsky, K., Skourup, H., Rinne, E., Parsakhoo, Z. S., Djepa, V.,  
11 Wadhams, P., and Sandven, S.: The impact of snow depth, snow density and ice density on  
12 sea ice thickness retrieval from satellite radar altimetry: results from the ESA-CCI Sea Ice  
13 ECV Project Round Robin Exercise, *The Cryosphere*, 9, 37-52, doi:10.5194/tc-9-37-2015,  
14 2015.

15 Kwok, R.: Sea ice concentration estimates from satellite passive microwave radiometry and  
16 openings from SAR ice motion, *Geophys. Res. Lett.*, 29, 9, doi:10.1029/2002GL014787,  
17 2002.

18 Kwok, R., Comiso, J. C., Martin, S., and Drucker, R.: Ross Sea polynyas: Response of ice  
19 concentration retrievals to large areas of thin ice, *J. Geophys. Res.*, 112, C12012,  
20 doi:10.1029/2006JC003967, 2007.

21 Mäkynen, M. and Similä, M.: Thin Ice Detection in the Barents and Kara Seas With AMSR-E  
22 and SSMIS Radiometer Data, *IEEE T. Geosci. Remote*, IEEE Early Access Articles, DOI:  
23 10.1109/TGRS.2015.2416393, 2015.

24 Mäkynen, M., Kern, S., Rösel, A., and Pedersen, L.T.: On the Estimation of Melt Pond  
25 Fraction on the Arctic Sea Ice With ENVISAT WSM Images, *IEEE T. Geosci. Remote*, 52,  
26 7366–7379, 2014.

27 Marcq, S. and Weiss, J.: Influence of sea ice lead-width distribution on turbulent heat transfer  
28 between the ocean and the atmosphere, *The Cryosphere*, 6, 143-156, DOI: 10.5194/tc-6-143-  
29 2012, 2012.

1 Markus, T., and Cavalieri, D. J.: An enhancement of the NASA Team sea ice algorithm, IEEE  
2 Trans. Geosci. Remote Sens., 38, 1387–1398, 2000.

3 Meier, W., and Notz, D.: A note on the accuracy and reliability of satellite-derived passive  
4 microwave estimates of sea-ice extent. CLIC Arctic sea ice working group. Consensus  
5 document, CLIC International Project Office, Tromsø, Norway, 28 October 2010.

6 Meissner, T., and Wentz, F. J.: The emissivity of the ocean surface between 6 - 90 GHz over a  
7 large range of wind speeds and Earth incidence angles, IEEE Transactions on Geoscience and  
8 Remote Sensing, 50(8), 3004-3026, 2012

9 Naoki, K., Ukita, J., Nishio, F., Nakayama, M., Comiso, J. C., and Gasiewski, A: Thin sea ice  
10 thickness as inferred from passive microwave and in situ observations, J. Geophys. Res., 113,  
11 2156-2202, 2008.

12 Njoku, E. G.: Nimbus-7 SMMR Pathfinder Brightness Temperatures. 25 October 1978–20  
13 August 1987, NASA DAAC at the National Snow and Ice Data Center, NASA, Boulder,  
14 Colorado, USA, 2003.

15 Notz, D. and Marotzke, J.: Observations reveal external driver for Arctic sea-ice retreat.  
16 Geophys. Res. Lett., 39, L08502, doi: 10.1029/2012GL051094, 2012.

17 NSIDC (National Snow and Ice Data Center): Monthly Ocean Masks and Maximum Extent  
18 Masks, [http://nsidc.org/data/smmr\\_ssmi\\_ancillary/ocean\\_masks.html](http://nsidc.org/data/smmr_ssmi_ancillary/ocean_masks.html)

19 Oelke, C., Atmospheric signatures in sea ice concentration estimates from passive  
20 microwaves: modelled and observed, Int. J. Rem. Sens., 18(5), 1113-1136, 1997.

21 Parkinson, C. L., and Cavalieri, D. J.: Antarctic sea ice variability and trends, 1979–2010, The  
22 Cryosphere, 6, 871–880, doi:10.5194/tc-6-871-2012, 2012.

23 Parkinson, C. L., Comiso, J. C., and Zwally, H. J.: Nimbus-5 ESMR Polar Gridded Sea Ice  
24 Concentrations, 1978-2011, edited by: Meier, W. and Stroeve, J., NASA DAAC at the  
25 National Snow and Ice Data Center, NASA, Boulder, Colorado USA, 2004.

26 Pedersen, L.T.: Merging microwave radiometer data and meteorological data for improved  
27 sea ice concentrations, EARSeL Adv. in Remote Sens., 3, 81-89, 1994.

28 Ramseier, R. O.: Sea Ice Validation, in: DMSP special sensor microwave/imager  
29 calibration/validation, edited by: Hollinger, J. P., Naval Research Laboratory, Washington,  
30 D.C, 1991.

- 1 Röhrs, J., and Kaleschke, L.: An algorithm to detect sea ice leads by using AMSR-E passive  
2 microwave imagery, *The Cryosphere*, 6, 343-352, doi:10.5194/tc-6-343-2012, 2012.
- 3 Röhrs, J., Kaleschke, L., Bröhan, D., and Siligam, P. K.: Corrigendum to "An algorithm to  
4 detect sea ice leads by using AMSR-E passive microwave imagery" published in *The*  
5 *Cryosphere*, 6, 343–352, 2012, *The Cryosphere*, 6, 365-365, doi:10.5194/tc-6-365-2012,  
6 2012.
- 7 Rösel, A., Kaleschke, L., and Birnbaum, G.: Melt ponds on Arctic sea ice determined from  
8 MODIS satellite data using an artificial neural network, *The Cryosphere*, 6, 431-446,  
9 doi:10.5194/tc-6-431-2012, 2012a.
- 10 Rösel, A., Kaleschke, L., and Kern, S.: Influence of melt ponds on microwave sensor's sea ice  
11 concentration retrieval algorithms, *Proceedings Geoscience and Remote Sensing Symposium*  
12 *(IGARSS)*, 2012 IEEE International, 23-27 July 2012, Munich, 2012b.
- 13 Scott, K. A., Buehner, M., and Carrieres, T.: An Assessment of Sea-Ice Thickness Along the  
14 Labrador Coast From AMSR-E and MODIS Data for Operational Data Assimilation, *IEEE T.*  
15 *Geosci. Remote*, 52, 2726–2737, doi: 10.1109/TGRS.2013.2265091, 2014.
- 16 Shokr, M., Lambe, A., and Agnew, T.: A new algorithm (ECICE) to estimate ice  
17 concentration from remote sensing observations: an application to 85-GHz passive microwave  
18 data, *IEEE T. Geosci. Remote*, 46, 4104–4121, doi: 10.1109/TGRS.2008.2000624, 2008.
- 19 Smith, D. M.: Extraction of winter total sea-ice concentration in the Greenland and Barents  
20 Seas from SSM/I data, *Int. J. Remote Sens.*, 17, 2625–2646, 1996.
- 21 Svendsen, E., Kloster, K., Farrelly, B., Johannessen, O. M., Johannessen, J. A., Campbell, W.  
22 J., Gloersen, P., Cavalieri, D., and Matzler, C.: Norwegian Remote Sensing Experiment'  
23 Evaluation of the Nimbus 7 Scanning Multichannel Microwave Radiometer for Sea Ice  
24 Research, *J. Geophys. Res.*, 88, 2781-2791, 1983.
- 25 Swift, C., Fedor, L., and Ramseier, R.: An Algorithm to Measure Sea Ice Concentration With  
26 Microwave Radiometers, *J. Geophys. Res.*, 90, 1087–1099, 1985.
- 27 Tonboe, R. T.: The simulated sea ice thermal microwave emission at window and sounding  
28 frequencies. *Tellus A*, 62, 333-344, 2010.

1 Tonboe, R. T., and Andersen, S.: Modelled radiometer algorithm ice concentration sensitivity  
2 to emissivity variations of the Arctic sea ice snow cover, Danish Meteorological Institute  
3 Scientific Report 04-03, Danish Meteorological Institute, Copenhagen, Denmark, 2004.

4 Tonboe, R. T., Dybkjær, G., and Høyer, J. L.: Simulations of the snow covered sea ice surface  
5 temperature and microwave effective temperature. *Tellus A*, 63, 1028-1037, 2011.

6 Tschudi, M. A., Maslanik, J. A., and Perovich, D. K.: Derivation of melt pond coverage on  
7 arctic sea ice using MODIS observation, *Remote Sens. Environ.*, 112, 2605–2614, 2008.

8 Ulaby, F. T., Moore, R. K., and A. K. Fung 1986. *Microwave Remote Sensing. Active and*  
9 *Passive*. Norwood, MA: Artech House Inc, 1986.

10 Wentz, F. J.: A well-calibrated ocean algorithm for SSM/I. *J. Geophys. Res.*, 102, 8703-8718,  
11 1997.

12 Wentz, F. J., Ricciardulli, L., Hilburn, K. A., and Mears, C. A.: How Much More Rain Will  
13 Global Warming Bring?, *Science*, 317, 233-235, 2007.

14 Willmes, S., Nicolaus, M., and Haas, C.: The microwave emissivity variability of snow  
15 covered first-year sea ice from late winter to early summer: a model study, *The Cryosphere*, 8,  
16 891–904, doi:10.5194/tc-8-891-2014, 2014.

17  
18  
19  
20  
21  
22  
23  
24  
25  
26  
27  
28

1 Table 1. The SIC algorithms shown in this study.

Algorithm	Acronym	Reference	Channels
Bootstrap P	BP	Comiso, 1986	37V, 37H <i>P</i>
CalVal	CV	Ramseier, 1991	19V, 37V <i>F</i>
Bristol	BR	Smith, 1996	19V, 37V, 37H <i>PF</i>
NASA Team	NT	Cavalieri et al., 1984	19V, 19H, 37V <i>PF</i>
<b>ASI</b>	ASI	Kaleschke et al., 2001	85V, 85H <i>P</i>
<b>Near 90GHz linear</b>	N90	Ivanova et al., 2013	85V, 85H <i>P</i>
ESMR	ESMR	Parkinson et al., 2004	19H
6H	6H	Pedersen, 1994	6H
ECICE	ECICE	Shokr et al., 2008	19V&19H or 37V&37H <i>P</i>
<b>NASA Team 2</b>	NT2	Markus and Cavalieri, 2000	19V, 19H, 37V, 85V, 85H <i>PF</i>
NT+CV	NT+CV	Ivanova et al., 2013	19V, 19H, 37V <i>PF</i>
<b>CV+N90</b>	CV+N90	Ivanova et al., 2013	19V, 37V, 85V, 85H <i>PF</i>
OSISAF	OSISAF	Eastwood (ed.), 2012	19V, 37V, 37H <i>PF</i>

2 *P* indicates that the algorithm is based on the polarisation difference or ratio at a single frequency; *F* indicates  
3 that the algorithm uses two different frequencies at the same polarisation (i.e., a spectral gradient). The names of  
4 the high-frequency algorithms (and the algorithms partially using high frequencies) are shown in bold, while the  
5 rest are low-frequency algorithms.

6

7 Table 2a. SIC SD (in %). Low SIC: 15% (0% for SMMR), winter (W) and summer (S). No  
8 open water filter applied. Ref – SD for the full SIC 0% dataset.

Northern Hemisphere								
		AMSR-E		SSM/I		SMMR		
Algorithm	Avg SD	S	W	S	W	S	W	Ref
6H	2.8	2.0	2.5			2.8	3.8	3.0
CV	3.8	3.6	3.5	4.6	3.8	3.5	3.9	4.8

NT+CV	4.5	4.6	4.4	5.1	4.6	3.9	4.2	5.5
OSISAF	4.7	5.3	4.8	5.4	4.7	3.8	4.1	5.2
NT	5.4	5.8	5.5	5.9	5.5	4.7	4.8	6.6
BR	6.6	7.1	6.7	6.6	6.1	6.4	6.4	7.8
ESMR	7.2	7.6	7.0	7.9	6.9	7.1	6.5	
NT2	7.3	6.3	6.7	8.9	7.2			
ECICE	9.4	10.7	10.0	8.8	8.2			
BP	13.5	14.5	13.1	12.4	11.4	15.2	14.1	15.5
CV+N90	15.8	15.6	15.6	16.5	15.3			19.8
ASI	28.5	31.3	30.1	27.0	25.7			
N90	28.8	28.9	28.8	29.6	27.8			35.9
<b>Southern Hemisphere</b>								
		<b>AMSR-E</b>		<b>SSM/I</b>		<b>SMMR</b>		
Algorithm	Avg SD	S	W	S	W	S	W	Ref
6H	2.2	2.1	2.4			1.9	2.2	2.3
CV	3.5	3.4	3.4	3.9	4.0	3.0	3.2	3.9
NT+CV	3.9	3.9	3.9	4.4	4.5	3.1	3.4	4.4
OSISAF	4.3	4.8	4.8	4.9	5.0	3.2	3.4	4.3
NT	4.4	4.6	4.6	5.0	5.2	3.4	3.7	5.0
BR	6.1	6.7	6.5	6.3	6.2	5.5	5.7	6.9
NT2	6.2	6.3	6.3	6.2	6.0			
ESMR	6.7	7.3	7.1	6.9	6.9	6.0	6.1	
ECICE	9.8	11.1	10.7	8.8	8.5			
BP	16.2	17.0	16.2	14.4	14.1	17.6	18.0	17.7
CV+N90	18.9	20.5	19.8	18.0	17.5			22.0

ASI	28.9	32.5	31.1	26.3	25.6			
N90	35.0	38.4	36.9	32.7	32.0			40.8

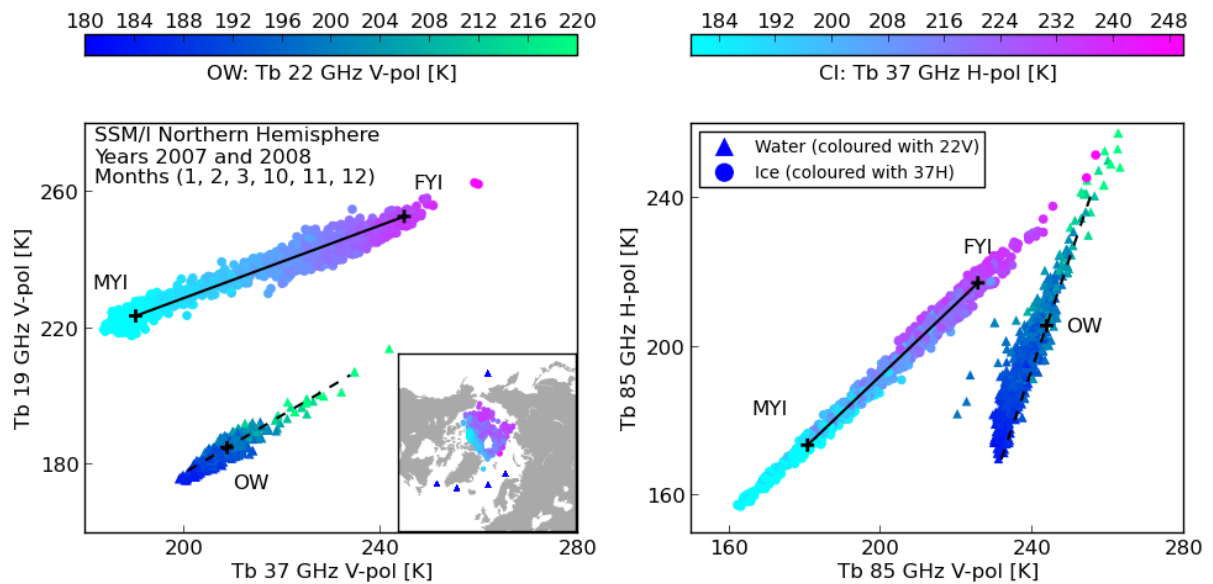
1

2 Table 2b. SIC SD (in %). High SIC: 75%, winter. No open water filter applied. Ref – SD for  
3 the full SIC 100% dataset.

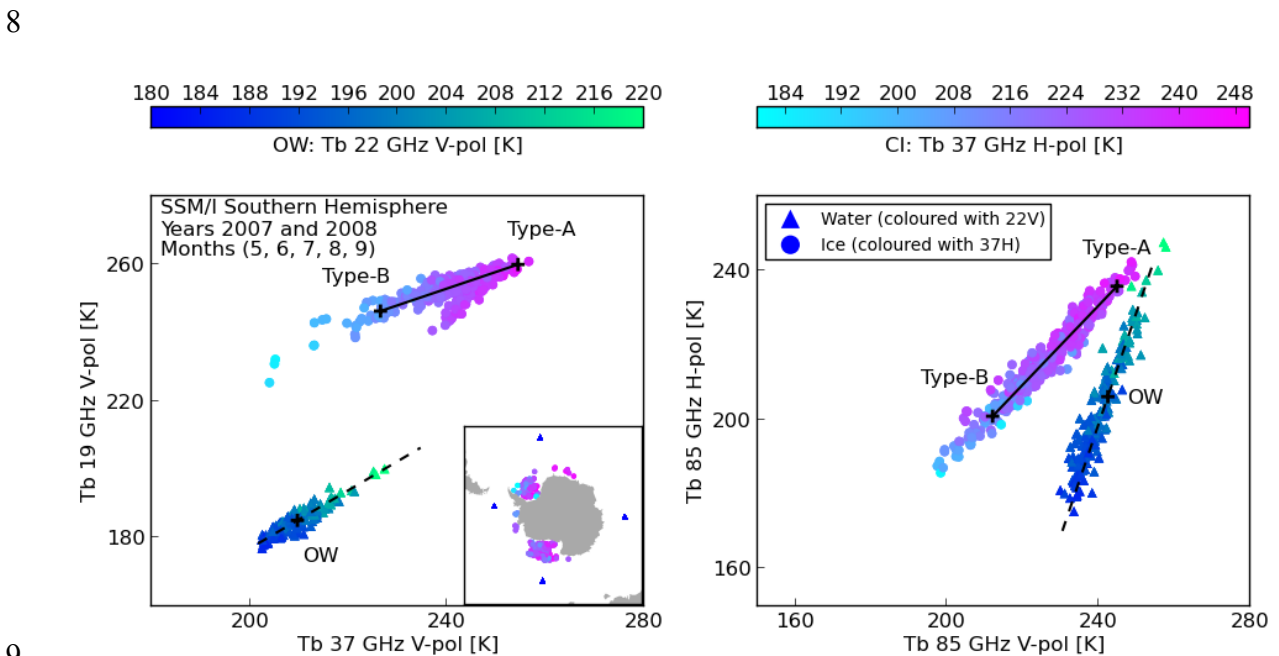
Northern Hemisphere					Southern Hemisphere				
Alg	Avrg SD	AMSR-E	SSM/I	Ref	Alg	Avrg SD	AMSR-E	SSM/I	Ref
BR	3.1	3.1	3.1	4.3	BR	2.9	2.8	3.0	4.5
OSISAF	3.1	3.1	3.1	4.3	OSISAF	2.9	2.8	3.0	4.5
NT+CV	3.1	3.1	3.2	4.4	6H	2.9	2.9		4.8
CV+N90	3.4	3.3	3.5	4.6	NT+CV	3.0	2.8	3.1	4.7
NT2	3.7	3.9	3.6		CV	3.4	3.0	3.7	5.4
6H	3.7	3.7		5.4	NT	4.3	4.2	4.4	6.6
NT	3.8	4.0	3.7	5.7	CV+N90	4.6	4.8	4.5	5.9
ASI	3.9	4.7	3.5		ECICE	4.9	5.4	4.6	
CV	4.5	4.5	4.5	6.4	ASI	4.9	5.9	4.3	
BP	4.6	5.2	4.3	6.2	NT2	5.8	5.7	5.8	
ESMR	4.7	3.0	5.4		ESMR	7.1	3.9	8.6	
N90	5.4	5.2	5.5	7.0	N90	8.1	8.4	7.9	10.4
ECICE	8.1	7.4	8.5		BP	9.0	8.7	9.2	13.1

4

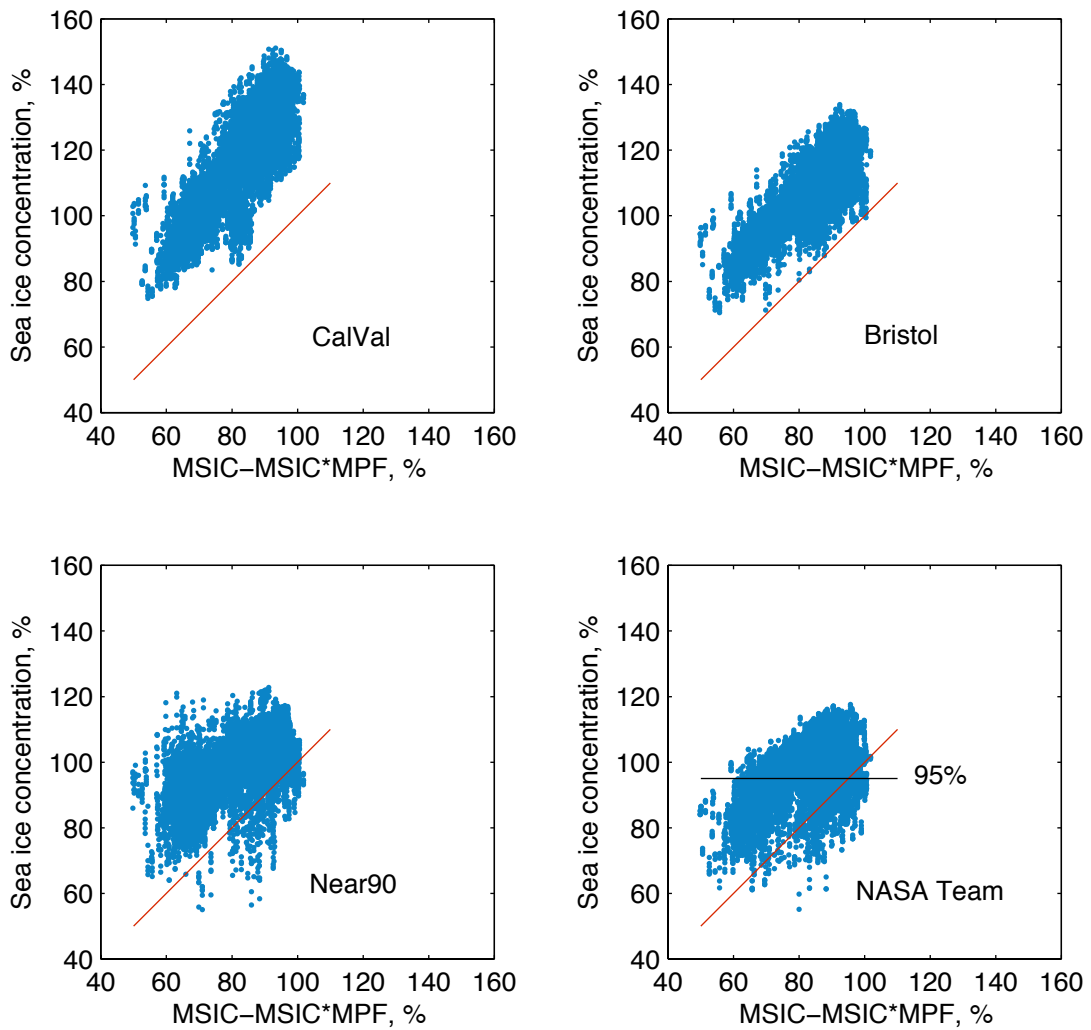
5



1  
 2 Figure 1. Coverage graphs for the SSM/I subset of the Northern Hemisphere RRDP in winters  
 3 2007 and 2008. Both the Tb and spatial coverage are displayed. In all panels, triangle symbols  
 4 are used for the OW locations, and circles for CI. In the Tb diagrams, the OW symbols are  
 5 coloured according to Tb22v values (left colour scale), while the CI symbols are coloured  
 6 according to Tb37h values (right colour scale). The colouring of CI symbols is also used in  
 7 the embedded map. Solid and dashed lines show ice and OW lines respectively.

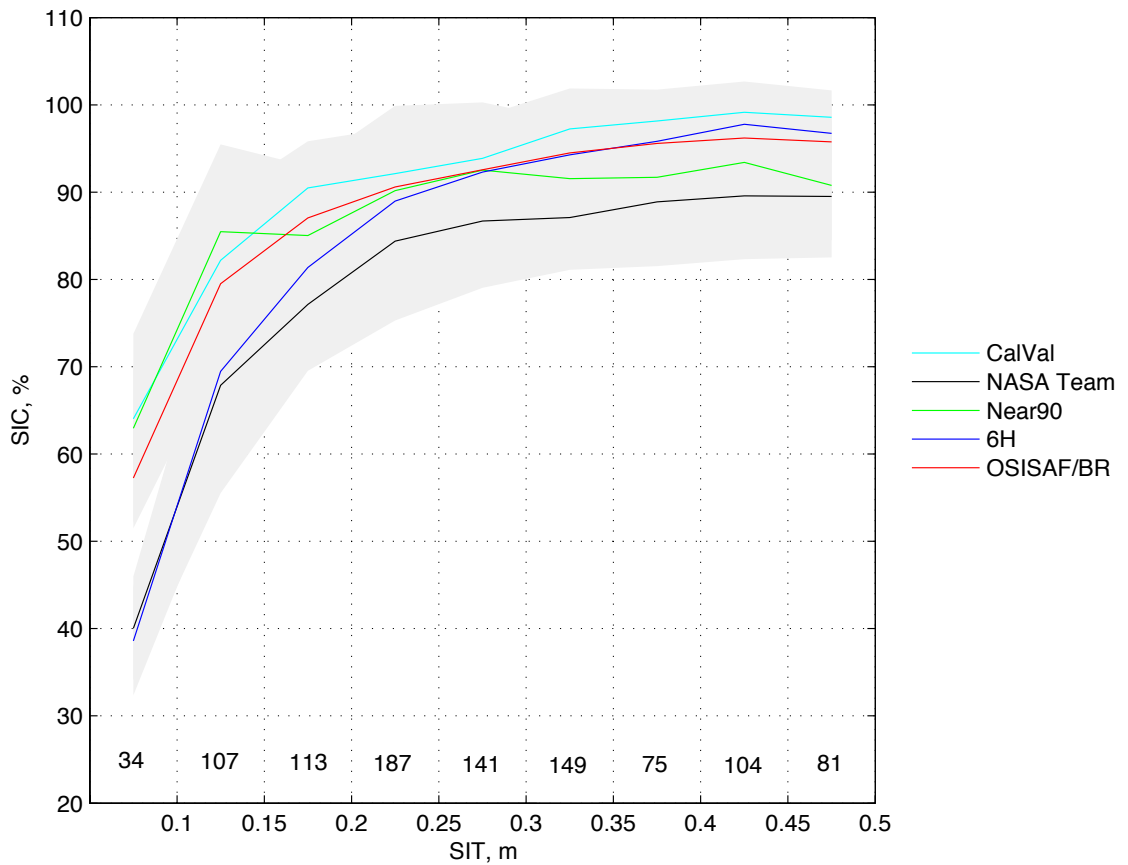


9  
 10 Figure 2. Same as Fig. 1, but in the Southern Hemisphere.



1

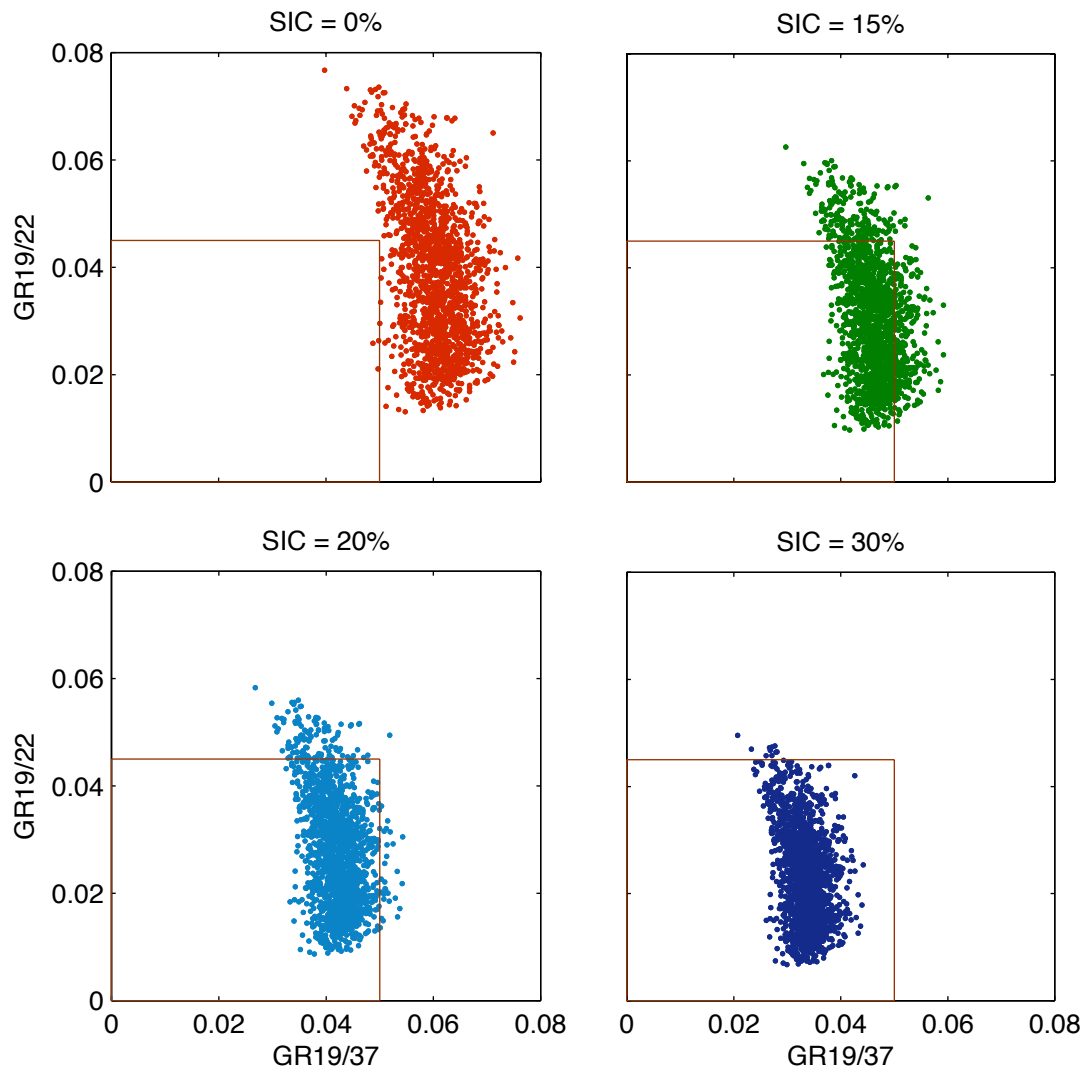
2 Figure 3. AMSR-E SIC in % (y-axis) obtained by four algorithms for the Arctic Ocean as a  
 3 function of the net ice surface fraction obtained by MODIS for 21 June – 31 August 2009.  
 4 The red lines show the one-to-one regressions. The black line shows the 95% SIC for NT (the  
 5 limit used for the dynamic ice tie point).



1

2 Figure 4. SIC calculated by the SIC algorithms as a function of SMOS ice thickness in areas  
 3 of the Arctic Ocean, which are known to be ~100% thin ice during the time period from 1  
 4 October to 12 December 2010. Grey shading shows SDs of the algorithms. Number of  
 5 measurements in each bin is shown above the x-axis (total number is 991). In this SIC range  
 6 OSISAF is the same as BR.

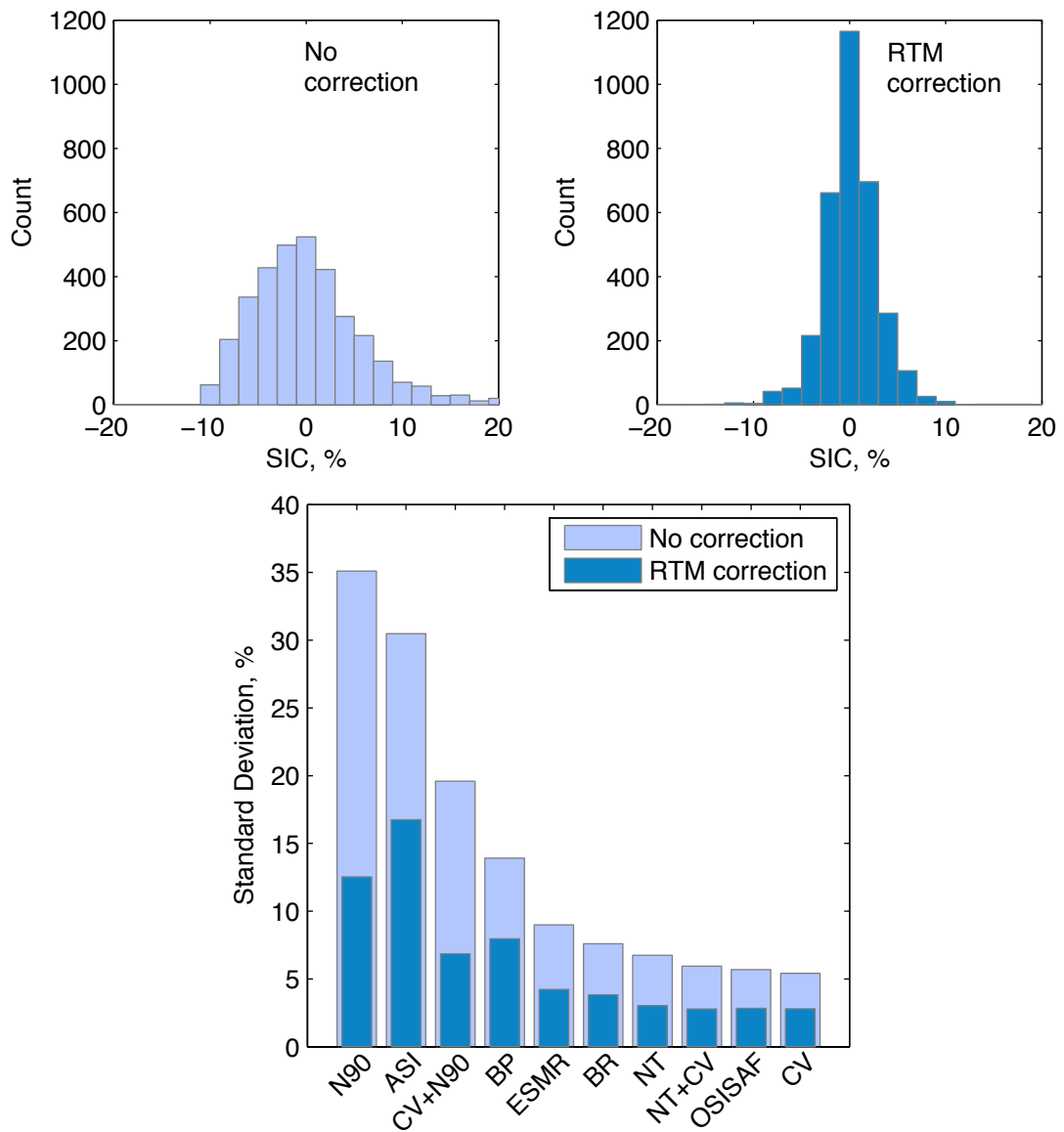
7



1

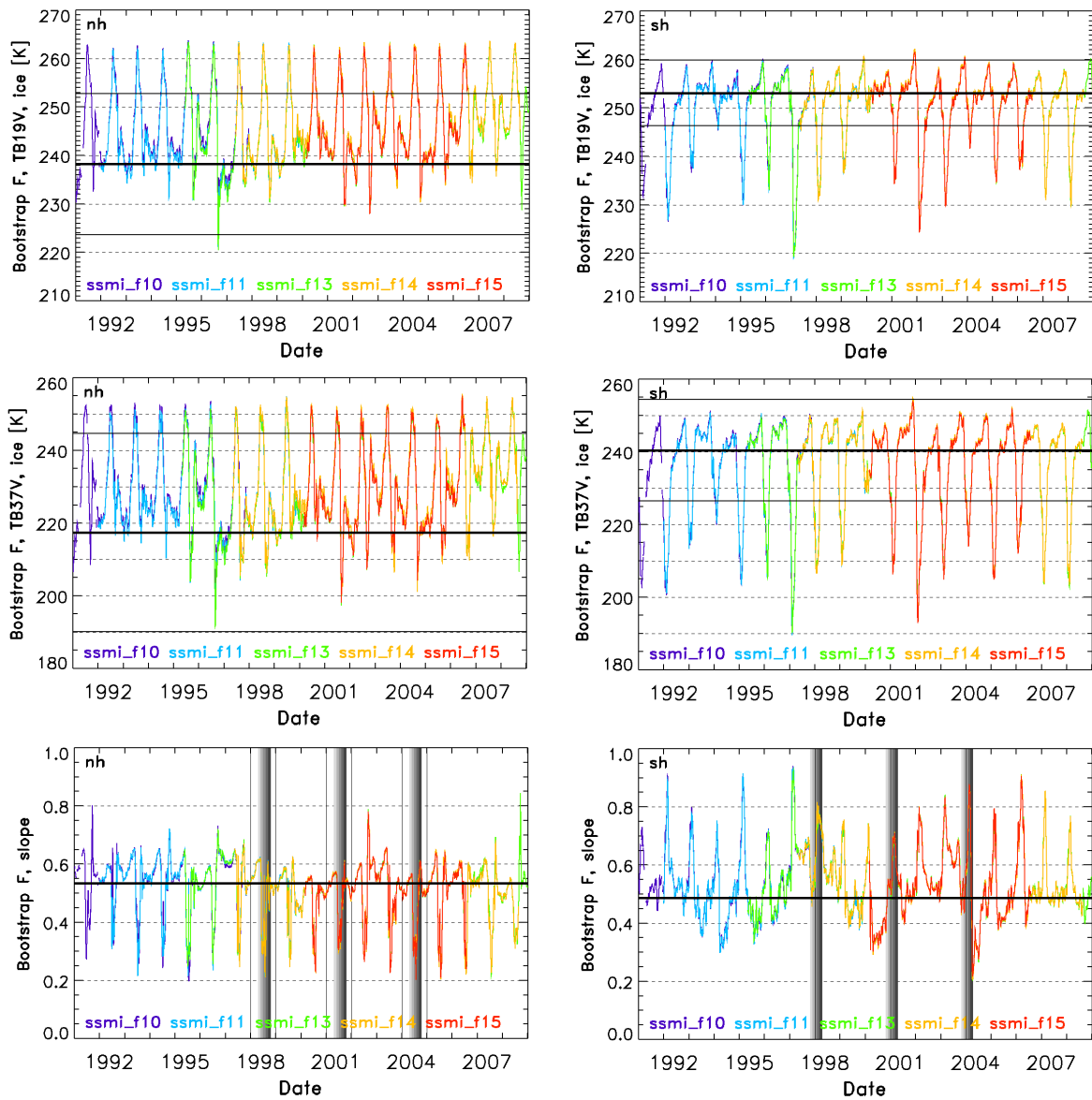
2 Figure 5. Demonstration of the open water/weather filter performance: gradient ratio (GR)  
 3 19/22 is plotted as a function of GR19/37 for SSM/I data in 2008 (entire year) for the  
 4 Northern Hemisphere for SIC of 0%, 15%, 20% and 30%. The red square shows the value  
 5 range outside which the open water/weather filter sets SIC values to 0% (open water).

6



1

2 Figure 6. Histograms SSM/I SIC obtained by the OSISAF algorithm over open water (SIC =  
 3 0%) in the Northern Hemisphere in 2008 (entire year) without correction (upper panel, left)  
 4 and with RTM correction (upper panel, right). The histograms contain 21 bins of 2% SIC.  
 5 Bottom plot: decrease in SDs for 10 SIC algorithms due to the atmospheric correction of the  
 6 measured Tbs.



1  
 2 Figure 7. Examples of tie points time series for the Bootstrap F algorithm in the Northern (left  
 3 panels) and Southern (right panels) hemispheres: Tb19v and Tb37v ice tie points (upper and  
 4 middle plots respectively) and slopes (bottom plots). The vertical bars in light grey to dark  
 5 grey colours denote the progressing melt season from May to September in the Northern and  
 6 from November to March in the Southern hemisphere.

7

8